TRIUMF

ANNUAL REPORT
SCIENTIFIC ACTIVITIES
2003

ISSN 1492-417X

CANADA'S NATIONAL LABORATORY
FOR PARTICLE AND NUCLEAR PHYSICS

OPERATED AS A JOINT VENTURE

MEMBERS:

THE UNIVERSITY OF ALBERTA
THE UNIVERSITY OF BRITISH COLUMBIA
CARLETON UNIVERSITY
SIMON FRASER UNIVERSITY
THE UNIVERSITY OF VICTORIA

ASSOCIATE MEMBERS:

THE UNIVERSITY OF GUELPH
THE UNIVERSITY OF MANITOBA
McMASTER UNIVERSITY
L'UNIVERSITÉ DE MONTRÉAL
QUEEN'S UNIVERSITY
THE UNIVERSITY OF REGINA
THE UNIVERSITY OF TORONTO

UNDER A CONTRIBUTION FROM THE
NATIONAL RESEARCH COUNCIL OF CANADA

DECEMBER 2004

The contributions on individual experiments in this report are outlines intended to demonstrate the extent of scientific activity at TRIUMF during the past year. The outlines are not publications and often contain preliminary results not intended, or not yet ready, for publication. Material from these reports should not be reproduced or quoted without permission from the authors.

PARTICLE PHYSICS

Experiment 614
TWIST – the TRIUMF weak interaction symmetry test
(B. Shin, TRIUMF)

TWIST is an experiment to measure the muon decay spectrum, to extract precise values of the decay (Michel) parameters, ρ, δ, and ξ [Michel, Proc. Phys. Soc. **A63**, 514 (1950)]. If the results differ from the standard model (SM) prediction [Fetscher and Gerber in *Advanced Series in Directions in High Energy Physics*, ed. P. Langacker (World Scientific, Singapore, 1995) v.14, p.657], the deviations indicate contributions from physics beyond the SM. The goal of TWIST is to simultaneously determine these decay parameters with experimental precison better than 10^{-3}, to eventually achieve approximately a tenfold improvement over the existing precision, shown in Table I along with theoretical SM predictions. When this goal is met, it will set new limits on the right-handed coupling of the muon in a model independent way, as well as squeeze the parameter space for certain classes of extensions to the SM.

The TWIST collaboration began to collect data in late 2002. During that first running period, measurements were made with the goal of providing an initial measurement of the ρ and δ parameters, as well as investigating systematic dependences and sensitivities to many different experimental variables.

Following the collection of about 6×10^9 events during that time, the simulation and various analysis codes, including the newly developed blind analysis code, were tested and validated in 2003. The availability of the WestGrid facilty has enabled us to compare high statistics analyses of combinations of many experimental and Monte Carlo (MC) data sets. Comparisons of the GEANT3-based MC program currently in use with GEANT4 have begun in the year, and a more detailed study is continuing.

We have also improved the functionality and reliability of the M13 beam line, established an improved beam tune, and extended the region of the spectrometer magnetic field map. As a result of analysis of the 2002 data where the muon stopping target was 125 μm mylar, the target was changed to a 71 μm, 99.99% pure Al foil.

Table I. Theoretical and measured values of the muon decay parameters.

	SM(V-A)	PDG currrent value
ρ	3/4	0.7518 ± 0.0026
η	0	-0.007 ± 0.013
δ	3/4	$0.7486 \pm 0.0026 \pm 0.0028$
$\mathcal{P}_\mu\xi$	1	$1.0027 \pm 0.0079 \pm 0.0030$

Brief description of the TWIST spectrometer

The spectrometer is designed to measure simultaneously ρ, δ, and $\mathcal{P}_\mu\xi$, where $\mathcal{P}_\mu$ is the muon polarization at the time of decay. The expected precision is such that the result will be about one order of magnitude better than the currently available best results, limited by systematic effects. Muons are stopped in a thin target at the centre of a stack of 56 low-mass, high-precision planar wire chambers in a uniform solenoidal field of 2 T. Each detector plane has a thickness of only about 5×10^{-5} radiation lengths, an important feature of the TWIST detector. The stack is shown in Fig. 1. Different types of wire chamber detector planes are employed and compared in Table II.

PCs serve to identify the primary characteristics of an event and to identify the times of each track with respect to a simple thin scintillator event trigger. The four PC planes at each of the upstream and downstream ends of the stack identify decay positrons as well as beam positrons. The four PC planes surrounding the stopping target (PC(t) in Table II) define the end of the incoming muon track. DCs use a much slower gas to achieve better position resolution. Their function is to determine precisely the coordinates of the decay positron path.

Table II. Description of DC, PC and target PC (PC(t)) chambers.

	DC	PC	PC(t)
Planes	44	8	4
Wires/plane	80	160	48
Wire spacing	4 mm	2 mm	2 mm
Gas	DME	CF_4/ iso-C_4H_{10}	CF_4/ iso-C_4H_{10}

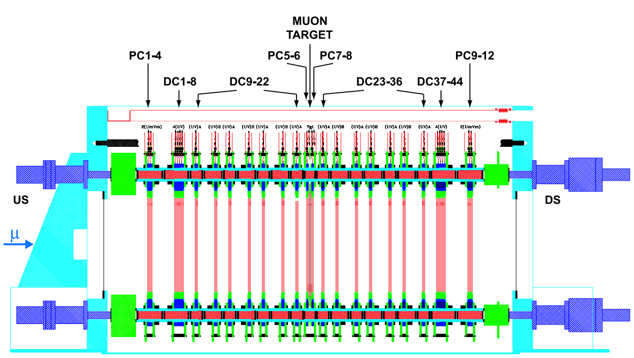

Fig. 1. Side view of the TWIST spectrometer detector stack.

The M13 beam

The M13 beam is a source of surface positive muons (μ^+), having a high degree of polarization in a direction opposite to the muon momentum ($\mathcal{P}_\mu \sim -1.0$) at production. However, the polarization at the stopping target is less than at the source, from real or apparent reductions due to known effects such as beam size and divergence, scattering from the materials along the beam line, and the fringe field of the spectrometer.

The most challenging measurement is $\mathcal{P}_\mu\xi$, for which the absolute polarization $\mathcal{P}_\mu$ of the muons at the time of decay must be known precisely. Most importantly, deviations from $\mathcal{P}_\mu = -1.0$ must be quantified in terms of systematic corrections. However, the possibility of an unknown source of small depolarization exists, so that a measurement of $\mathcal{P}_\mu\xi$ which is less than one might have to be interpreted as a lower limit.

Most depolarization effects related to beam transport can be minimized by using a small momentum acceptance, beam divergence and beam size. During 2003, these have been measured as a function of the beam line element settings (beam tune) using a movable slit and fast wire chambers, and a new tune has been established. For frequent monitoring of the beam size and divergence, a time expansion chamber (TEC) has been designed and constructed, and is being tested.

The stability and reproducibility of the beam line magnet power supplies was previously improved by installing precision direct current transformers. Plans were made for a further upgrade with installation of a new vacuum isolation valve at the first focus point of the beam line as well as a removable window valve to prevent radioactive residual gases from migrating from a graphite production target to the end of M13 and disrupting the TWIST detectors. The Be production target which has so far been used can then be replaced by a graphite target to improve beam characteristics. The solenoid field has been mapped to the position of the last quadrupole of the beam line, so that the fringe field depolarization can be estimated precisely.

Progress in software and analysis

Tracking decay positrons Tracking of decay positrons is very demanding for TWIST because of the low tolerance for biases from reconstruction errors. Consequently a great deal of effort has been allocated to optimization of tracking.

1. Crosstalk removal: Although it is not a substantial source of chamber noise, crosstalk is removed prior to event classification using primarily the time width of the chamber hit signals and the existence of a coincident generating signal.
2. Event classification: Temporal and spatial properties of the hits allow the classification of events. For example, a muon as the trigger particle can readily be distinguished from a beam positron trigger, while decay positrons following the muon are also easily recognized. Subsequently, many types of problematic events can be identified without bias.
3. Pattern recognition: Drift chamber hits are sorted into temporal groups for which initial helix parameters are calculated from the positions of clusters of wire hits. Two independent routines have been written and compared, both statistically and by visual event screening. At present, reconstruction failures are at the 1% level.
4. Delta identification: Once hits are assigned to tracks, associated low energy tracks (deltas) can be identified and removed. Delta identification is a very important validation of the simulation, because we rely on the simulation to account for deltas produced below our detection threshold. Comparisons show that the number of deltas removed from the data is consistent with simulation.
5. Tracking: A least squares procedure is used to fit to the wire centres of the hits using the "narrow windows" method, which also resolves most left-right ambiguities. Drift time fits to overcome limitations of the wire centre fits (especially the granularity of the detector resolution function) were implemented. Multiple scattering (MS), which occurs mainly at the detector plane positions, is significant in the TWIST detector, especially for high angle tracks. To account for MS, kinks are introduced in the fitting function at the positions of the detector planes.
   The detector plane spacing of the inner DCs in TWIST causes the circle radius of some events to be undefined. However, for these difficult cases, the outer 8 DCs can be utilized since their plane spacing is much smaller. All wires in these planes were instrumented in the last year and are now used in tracking.
   There are several key tracking software development projects in progress which include: replacement of the uniform field by non-uniform fields, introduction of the variation of the resolution with distance from the wire in place of an averaged resolution function currently in use, and using a maximum likelihood fitter.

Calibrations Several calibration procedures have been refined. Calibration of the relative TDC times can now be done both with straight and helical tracks, and the accuracy of the energy calibration has been improved. The fitting of 120 MeV pion tracks in zero magnetic field has been complemented with the use of decay positron helices for determining translational and rotational alignments of chamber planes.

Simulation Improvements this year include the incorporation of a realistic distribution of charge clusters produced by ionization in the chambers, leading to reasonable simulation of the observed spatial resolution. Detector translational and rotational (mis)alignments have been included in the simulation. The phase space of the M13 beams used in 2002 was characterized this year and included as input. Additionally we have carried out a series of comparisons between the GEANT3 and GEANT4 packages to explore differences which might affect our results.

Computer cluster and grid computing Much of the development and testing of our analysis software has been accomplished using a local cluster of some 30 computers. In November, TWIST became a beta-tester of the WestGrid cluster of 1008 processors at UBC, allowing full scale simulation and data analysis. Submission scripts had to be revised significantly to conform with WestGrid disk storage architecture, while instabilities in the storage and queuing systems added additional complications. Nevertheless, access to this powerful system permitted generation and analysis of 15 Tbytes of simulation data, and analysis of much of both the 2002 and 2003 data sets (about 2.5 Tbytes). Twelve separate analyses were performed on a "standard" data set to study various analysis-dependent systematics.

Extraction of decay parameters and blind analysis

To extract decay parameters from the experimental energy and angle spectrum of decay positrons, there are two possible approaches: one is de-convoluting the measured spectrum to allow for direct comparison with the theoretical prediction, and the other is convoluting the theoretical shape with the detector response function and comparing to the experimental spectrum. The de-convolution method requires a precise knowledge of detector response function without which its application is impractical. The convolution, on the other hand, can be calculated directly by the MC simulation program without the explicit knowledge of detector response, but with a theoretical formula containing specific values of decay parameters.

To perform a fit for unknown values of decay parameters, TWIST has developed a technique which uses an expansion of the convoluted spectrum in deviations of the parameters from the values used as MC input. Assuming that the measured spectrum results from small deviations in the input values of decay parameters, the measured spectrum can be expressed near those values of the parameters by Taylor expansion up to the first order term, which is exact since the Michel form of the spectrum is linear in parameters ρ, η, ξ, and $\xi\delta$. Thus the measured spectrum is the sum of the MC spectrum assuming the input values, plus MC-generated derivative spectra multiplied by the differences between the input and measured parameters. The input values of the decay parameters are chosen randomly and are hidden, and only the deviations from the MC input values, not the decay parameters themselves, are given by the fit results. Experimenters remain "blind" to the parameters until the final result is determined. The MC simulated spectrum and the derivative distributions are obtained from *reconstructed* MC events; since TWIST uses the same reconstruction program for MC as for real data, any distortions introduced by the reconstruction software cancel exactly. The uncertainties come from how well the simulation recreates the real detector and the physics processes taking place.

During 2003 TWIST implemented and tested all parts of the blind analysis software chain, from the "black box" spectrum generator to the fitter. The tools have been checked with simulations and are now being used for fitting of experimental distributions. The system is also being applied to the estimation of biases and systematic effects.

Verification of simulation precision

TWIST results depend on the inherent and inevitable biases of experimental variables and analysis software. To minimize these biases, the physics content and implementation of the simulation can be compared with real data which are not sensitive to the decay distribution parameters. For this purpose the TWIST detector can be used for different kinds of verifications. A few that have so far been explored with the detector are listed here.

1. Muon stopping distribution: The muon range spread near the target will influence the energy calibration as well as muon depolarization. With external degradation of muon energy, the muon stopping distribution can be moved into the upstream half of the detector stack. Comparison of the stopping positions with simulated data tests the simulation of the energy loss as well as sensitivity of the observed range to small changes in the muon beam settings.

2. Response function and positron energy loss: Since the detector stack is made of two mirror-symmetric independent positron spectrometers, real decay positron tracks can be measured twice, once in each half of the stack, by arranging for muons to stop near either the entrance or exit of the spectrometer. Measurement of the difference of momentum and angle between the two halves, for both real data and simulated data, will show any weakness of the positron simulation and test not only how well the response function is reproduced but also how well the simulation

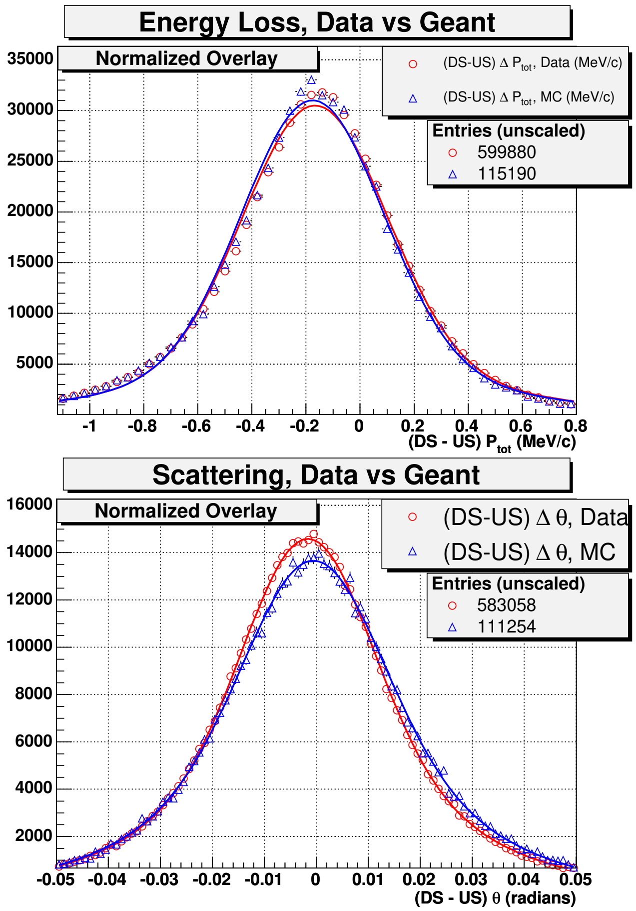

Fig. 2. Preliminary comparison of data and MC for decay positron tracks originating from muons stopping near the entrance to the stack. Top shows energy loss, and bottom shows multiple scattering. Circles are for data, and triangles for MC. The curves are simple two-component Gaussian fits, which are shown for comparison purposes only.

handles energy loss and multiple scattering of positrons in our fiducial range. Data taken with the stopping Al target in 2003 have been compared with simulation. A very preliminary result is shown in Fig. 2. The top graphs show that energy loss of less than 200 keV between the two halves is well reproduced by the simulation, while the Gaussian curves do not reproduce the shapes properly for either data or simulation. The bottom graph shows some disagreement with the simulation, which may be related to incomplete alignment of detector modules in the reconstruction program; a similar comparison for 2002 data, where a more complete alignment procedure was completed, does not show the difference.

3. Material asymmetries: If the simulation does not accurately generate secondary charged particles from positrons passing through and exiting the detector, there is a potential for bias in the decay parameters extracted from the comparison of real data with MC. This is most obvious in the angular distribution, since the number of secondaries produced varies approximately as $1/\cos(\theta)$. The beam entrance assembly of scintillators, vacuum tubes, flanges and windows, etc. is potentially a significant source of secondaries. To estimate how well the simulation reproduces these, comparisons of real data (with and without a disk of thickness 6.3 mm Al at the exit of the stack) with simulations show noticeable differences near $\cos(\theta) \approx 0.3$ as shown in Fig. 3. This is the most obvious weakness in the simulation, and efforts to identify its source are under way.

Tests and evaluations of systematic effects

TWIST accumulated several data sets in 2002, each large enough to determine ρ and δ with statistical precisions of about 10^{-3}. Two of these sets were accumulated in preferred conditions, i.e. optimum setting of experimental conditions at the time. Some fourteen other such sets were taken in which an experimental variable was modified or changed significantly beyond the normal control and/or monitoring range, so that the influence of each variable on the extracted Michel decay parameters could be studied. The altered variables included, among others, the solenoid field, the trigger (muon) rate, the μ stopping position, the field of the second bending dipole magnet in the beam line, the upstream/downstream material asymmetry, the voltages on the detectors, and the μ polarization. Some portions of these data sets were taken at different atmospheric pressures and temperatures so that systematic sensitivity to these environmental variables could be studied. Several small data sets were taken to add further information on the energy calibration and detector material thicknesses versus that in the MC simulation.

In 2003, some of the measurements described above have been repeated with a new M13 beam tune and a with an Al stopping target replacing the graphite-coated mylar target used in earlier runs. The high purity metal stopping target appears to reduce depolarization of the stopping muons, which could otherwise severely limit the sensitivity to the more fundamental effects on $\mathcal{P}_\mu\xi$ which TWIST hopes to explore. The usefulness of analogue information from the PCs near the the stopping target was also studied.

Examples of preliminary results

Two approximately equivalent experimental data sets (which we call Set A and Set B) were taken in 2002 with our preferred set of experimental variables. An initial WestGrid analysis of each one was compared with an identical analysis of a simulated spectrum plus derivative spectra using the blind analysis procedures. All three distributions were subjected to an independent end-point energy calibration, and the calibrated

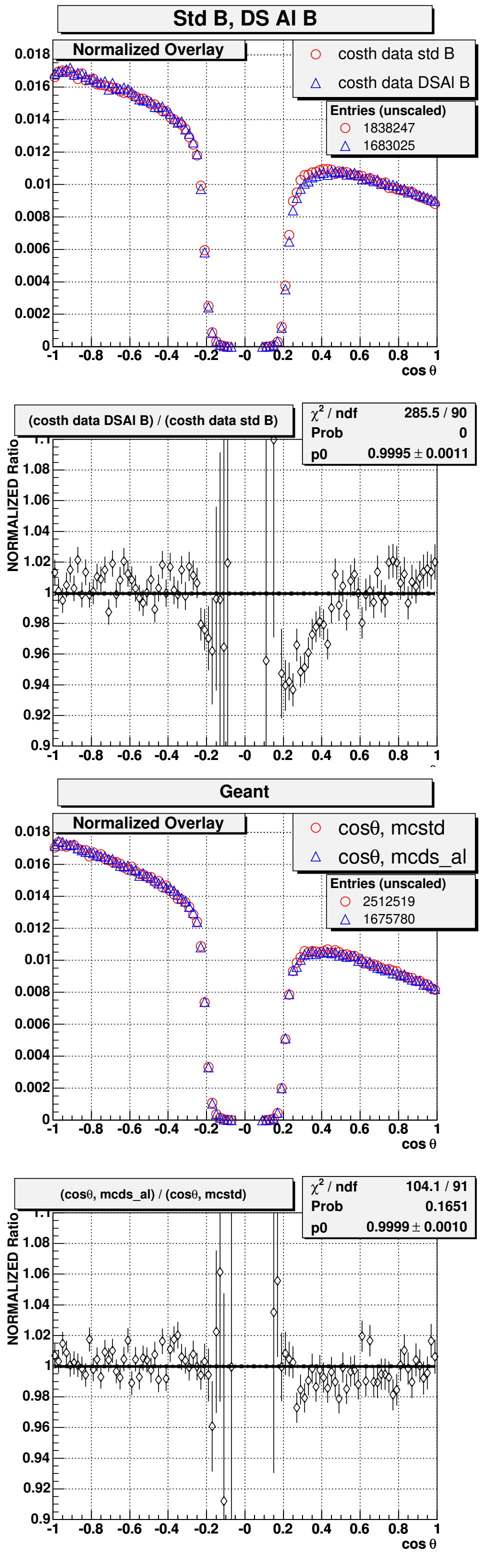

Fig. 3. Effect of the addition of a 6.3 mm thick Al plate at the DS exit of the detector stack, for data (upper two plots) and in the simulation (lower two plots). In both cases, one plot compares histograms where both have been scaled to a common number of entries (normalized overlay), while the other shows the differences by plotting the ratio of the normalized distributions.

data were binned in two dimensions. Within the very conservative fiducial range of $20 \leq p_e \leq 50$ MeV, and $0.54 \leq |\cos(\theta)| \leq 0.80$, the simulated base spectrum had about 1.4×10^7 events, while each experimental data set had about 1.0×10^7 events. The preliminary fit results shown in Table III were obtained. Improvements to these initial fits are continuing, with increased statistical precision of the simulations. A study of the optimum form and extent of the fiducial regions is also under way to determine a suitable compromise between sensitivity and statistics vs. systematic uncertainties.

Figure 4 shows plots of normalized residuals of the differences between the experimental and the MC data for momentum and $\cos(\theta)$ from fit results for Set A.

Table III. Preliminary results of blind analysis fits of simulated data to two experimental data sets. The values are differences from hidden decay parameters used by the simulation.

	Set A	Set B
$\Delta\rho(10^{-3})$	–12.7 ± 2.6	–14.2 ± 2.6
$\Delta\eta(10^{-1})$	–1.0 ± 1.4	–0.8 ± 1.4
$\Delta\mathcal{P}_\mu\xi(10^{-3})$	62.0 ± 2.6	61.8 ± 2.6
$\Delta\delta(10^{-3})$	–10.8 ± 1.4	–12.5 ± 1.4
χ^2/dof	1449/1556	1557/1556

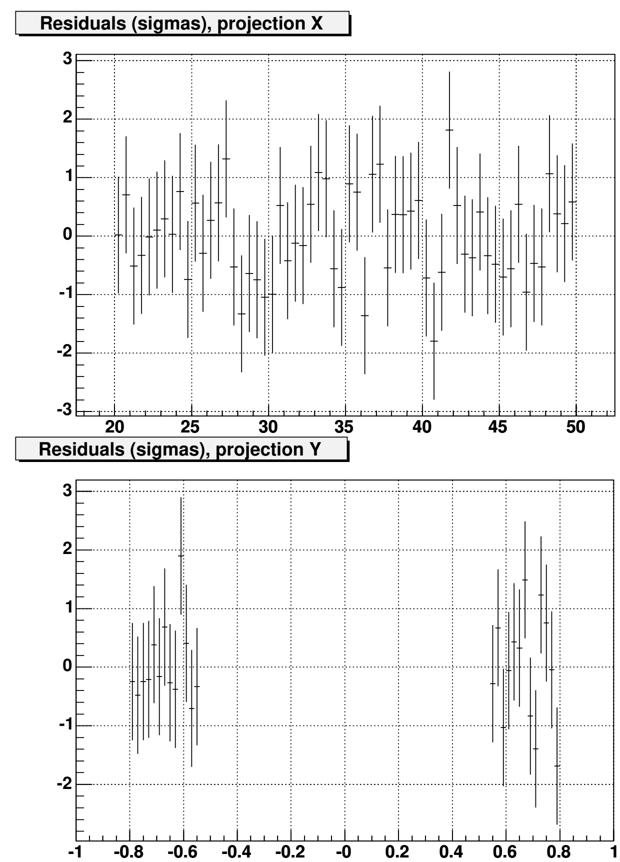

Fig. 4. Differences of experimental and simulated data in terms of normalized residuals of the two-dimensional fit, shown as projections in momentum (top) and $\cos(\theta)$ (bottom).

While the fit values, taken independently, are not particularly meaningful due to the hidden values of the simulated decay parameters, there is good agreement between the two experimental sets for all four parameters. The fit quality is very satisfactory. The statistical uncertainties, while not yet below the level of 10^{-3}, are close enough that we can say with confidence that we have enough experimental data to exceed this goal. The gains will come from an increase in simulation statistics, an expansion of the fiducial region, and a combination determined *a priori* of results of data sets taken under different conditions.

Summary

TWIST has achieved substantial progress in 2003. Problems which have been encountered either have been or are in the process of being solved. Data obtained so far appear to give the information necessary to provide ρ and δ at a precision of 10^{-3}. The WestGrid system satisfies our computing needs for this goal. Event reconstruction, data simulation, and fitting procedures are becoming mature and have passed many tests. The blind analysis procedure is proving to be extremely valuable for fitting of data to simulated distributions, and for evaluation of systematic effects between different data sets or different simulations in terms of precisely extracted values of decay parameters. Improvements to the muon beam, as well as our ability to control and measure it, are also continuing. All indications so far are that the goals of the experiment will be achieved, i.e. to attain at least an order of magnitude improvement in the existing uncertainties for ρ, δ, and $\mathcal{P}_\mu \xi$.

The ATLAS Experiment at the LHC

(C. Oram, TRIUMF)

As described in detail in the 1996 Annual Report, ATLAS is building a general purpose *pp* detector which is designed to exploit the full discovery potential of the Large Hadron Collider (LHC) at CERN. The TRIUMF group is responsible for the management and engineering of the hadronic endcap (HEC) calorimeters, and the feedthroughs for the endcap cryostats. For the HEC, this year has seen the insertion of the two wheels of the first endcap into their cryostat, and the assembly of the two wheels for the second (and final) endcap. The wheel assembly and cryostat insertion at CERN is led by a TRIUMF staff member.

Physics goals

The present theoretical understanding of elementary particles is in the context of the standard model. It is a remarkably successful model, providing predictions which have been consistently confirmed by experiments for over two decades. Its agreement with experimental results, to enormous accuracy in some cases, makes it the most accurately verified model in science. Of the many elementary particles contained in the standard model, only the Higgs remains to be discovered. The central goal of ATLAS is the search for the Higgs particle.

There are good theoretical reasons to believe that the discovery of the Higgs will at least contain hints at, and more likely direct evidence of, what lies beyond the standard model. If the Higgs is composite, its existence requires as yet unknown ultra-strong forces. If it is elementary, it would be the only spinless particle to be discovered so far. There is a theoretical "naturalness" problem for the masses of spinless particles. In the standard model, which is a highly nonlinear dynamical system, the elementary particles tend to take on the heaviest of all possible mass scales, which in such a model are at inaccessible energies and inconsistent with other requirements of the model. All other particles discovered thus far have natural mechanisms, such as gauge and chiral symmetries, for protecting their masses so that they can lie in the observable range. For the Higgs particle, there is no such symmetry in the present model. The only theoretical scenarios which leave the Higgs particle light enough to observe are hypothetical ones, either technicolour or supersymmetry, both radical departures from the present structure of the standard model. If the Higgs is observed at the LHC, one of these scenarios should be seen at the same time.

Particle theory has progressed enormously over the last few decades with many appealing scenarios for physics beyond the standard model. The most likely of these is supersymmetry and the boldest of these is superstring theory. These theories are intimately related and are both radical ideas which promise a new conceptual framework for understanding elementary particles. Though far from being complete theories at present, there are superstring models which resemble the standard model in their low energy limit. These models have a great appeal as they contain a unification of fundamental forces which includes gravity. They have already had substantial impact on gravitational physics where, for example, in addition to the long sought reconciliation of gravity with quantum mechanics, they have been used to derive a fundamental understanding of black hole thermodynamics. Superstring theory is still in its infancy, but progress has been dramatic and the promise of great things to come has captured the imagination of a substantial fraction of the world's theoretical particle physicists.

The present theoretical view is that the conventional grand unification of the strong, weak and electromagnetic forces can only work in the supersymmetric extension of the standard model. In that model, the grand unified energy scale is only two decades below the Planck scale, the ultimate energy where space-time itself has quantum fluctuations. It is not out of the realm of imagination that, at energy scales where supersymmetry would be observed, evidence for an ultimate theory of everything, or at least everything that can exist once space-time is formed, is within human grasp.

Experiments at the LHC, where the ATLAS detector will take data, will probe the energy region where the Higgs particle, possibly supersymmetry, or other structures will be visible. This will be the first experimental probe of an energy region in many years where fundamentally new physics is expected to occur . There is every reason to believe that the results will be among the most dramatic ever.

Basic ATLAS design considerations

The most prominent issue for the LHC is the quest for the origin of the spontaneous symmetry-breaking mechanism in the electroweak sector of the standard model. This is related to one of the most fundamental questions of physics: What is the origin of the different particle masses? New direct experimental insight is required to answer this question.

One of the possible manifestations of the spontaneous symmetry-breaking mechanism could be the existence of a standard model Higgs boson (H), or of a family of Higgs particles ($H^{\pm}$, h, H and A) when considering the minimal supersymmetric extension of the standard model (MSSM). The Higgs search is therefore used as a first benchmark for the detector optimization. For the SM Higgs, the detector has to be sensitive to the following processes ($\ell = e$ or μ) in order to cover the full mass range above the discovery limit set by the final LEP operation in the fall of 2000:

$H \to b\bar{b}$ from WH, ZH and $t\bar{t}H$ using a $\ell^{\pm}$ and b-tagging,
mass range $80 < m_H < 100$ GeV;

$H \to \gamma\gamma$
mass range $90 < m_H < 150$ GeV;

$H \to WW^* \to \ell^{\pm}\nu\ell^{\pm}\nu$
mass range $150 < m_H < 200$ GeV;

$H \to ZZ^* \to 4\ell^{\pm}$
mass range 130 GeV $< m_H < 2m_Z$;

$H \to ZZ \to 4\ell^{\pm}, 2l^{\pm} + 2\nu$
mass range $m_H > 2m_Z$;

$H \to WW, ZZ \to l^{\pm}\nu + 2$ jets, $2\ell^{\pm} + 2$ jets from WW, ZZ fusion using tagging of forward jets for m_H up to about 1 TeV.

In addition to signatures similar to these, the MSSM Higgs searches also require sensitivity to processes such as:

$$\begin{array}{lll} A \to \tau^+\tau^- & \to e\mu + \nu\text{'s} & \\ & \to \ell^{\pm} + \text{hadrons} + \nu\text{'s}; & \\ H^{\pm} \to \tau^{\pm}\nu & \text{from } t\bar{t} & \to H^{\pm}W^{\mp}b\bar{b} \text{ and} \\ \quad \to 2 \text{ jets} & \text{using a } \ell^{\pm} \text{ tag and } b\text{-tagging}\,. & \end{array}$$

The observable cross sections for most of these processes are small over a large part of the mass range to be explored at the LHC. Hence it is important to operate at high luminosity, and to maximize the detectable rates above backgrounds by high-resolution measurements of electrons, photons, and muons.

Figure 5 shows the estimated signal significance for the standard model Higgs discovery in ATLAS over the presently theoretically favoured region: 100–200 GeV/c^2. From 100–190 GeV/c^2, the most significant discovery channels are where the Higgs is produced by vector boson fusion [see Asai *et al.*, "Prospects for the search for a standard model Higgs boson in ATLAS using vector boson fusion", ATLAS Note SN-ATLAS-2003-24]. While the cross section for production is lower in these channels, the ability to cleanly tag the Higgs production by forward jets that enter the endcap calorimeters more than compensates, yielding superior signal to noise in these channels. The need to use the endcap calorimeters for this tag, puts a premium on obtaining an early robust calibration for the calorimeters over the entire angular range.

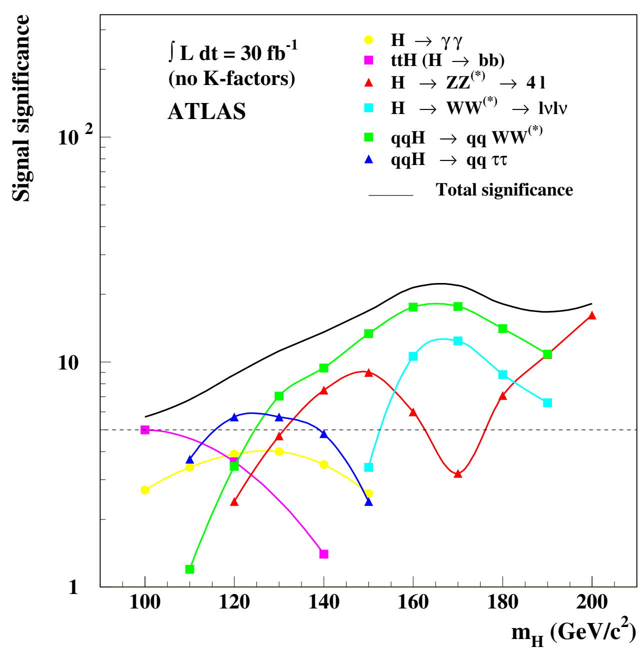

Fig. 5. ATLAS sensitivity for the discovery of a standard model Higgs boson for an integrated luminosity of 30 fb^{-1}. The signal significances are plotted for individual channels, as well as for the combination of all channels.

Canada's participation in ATLAS

The Canadian group consists of about 35 grant eligible physicists from TRIUMF, University of Alberta, Carleton University, Simon Fraser University, University of British Columbia, Université de Montréal, University of Toronto, University of Victoria, and York University. We are strongly involved in three construction projects centred around detecting hadrons in the endcap region: the hadronic endcap project, the hadronic portion of the forward calorimeter project, and the pipeline electronics for calorimetry. In addition, we are committed as part of our common project contribution to providing the feedthroughs for the two endcap cryostats. TRIUMF is directly involved in all of these projects, and in the physics simulations.

The hadronic endcap project

The hadronic endcap (HEC) calorimeter is a liquid argon sampling calorimeter with copper absorbers [ATLAS Collab., ATLAS Liquid Argon Technical Design Report (1996)]. A concise overview of this design was provided in the 1996 TRIUMF Annual Report. An artist's impression of a module can be seen in Fig. 6. Four detector systems sit in each endcap cryostat: nearest the interaction region is the presampler, followed by the electromagnetic endcap (EMEC) and the HEC. At the inner diameter around the beam pipe is the forward calorimeter (FCAL).

Hadronic endcap module production and testing By the end of 2002 we had constructed all the modules, and tested 120 of the 132 modules that constitute the two HEC endcaps in ATLAS. During 2003 the final 12 modules were successfully tested, bringing to an end the era of module production.

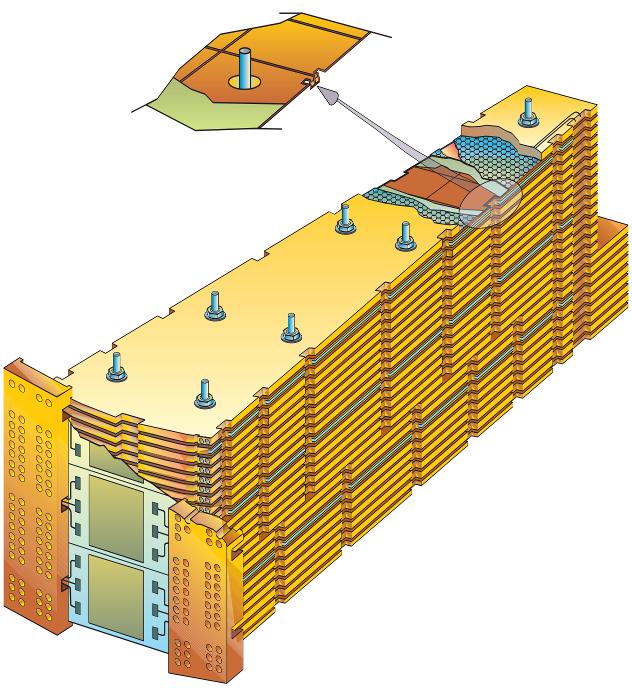

Fig. 6. Artist's impression of a hadronic endcap module.

Test beam measurements of the hadronic endcap modules This year we were preparing for the joint test of the three calorimeters in the endcap, scheduled for beam in 2004. During 2003, 16 purpose built small "inner radius" HEC modules were constructed in the HEC Russian Institutes, with full involvement of TRIUMF in design, materials procurement, and management. An engineering run of the test beam set-up is scheduled for February, 2004, with beam runs in the spring and fall of 2004. This test will use pre-existing EMEC and FCAL modules, along with these "inner radius" HEC modules.

In the summer of 2002, the combined performance of the HEC and EMEC series production modules was successfully tested in the H6 beam line at CERN. The H6 beam line provides beams from 20 to 180 GeV. During 2003 these data were successfully analyzed and a NIM article is presently in the final stages of preparation. This is an important step for the group as these measurements form the basis of the calibration of the calorimeter system as it will be used at LHC beam startup.

Wheel assembly at CERN A HEC wheel is formed from 32 modules. There are two wheels at each end of ATLAS, so we must assemble 128 modules into four wheels. The equipment for the wheel assembly is a Canadian responsibility. The four wheels and the two wheels of the EM calorimeter, which go into the same cryostat, are assembled in the horizontal orientation. Hence each wheel, which weighs about 90 tonnes, must be taken from its assembly table, rotated to the vertical and moved to the cryostat. This rotation and translation of equipment is also a Canadian responsibility. The engineering was undertaken by a collaboration between Alberta and TRIUMF personnel. The production of the equipment was by Canadian industry. This year saw the rotation of the first EM calorimeter wheel, and the successful insertion of the EM and HEC wheels into the cryostat, thus completing the first cryostat for the three large wheels (see Fig. 7). The two HEC wheels which will go into the second cryostat, have been assembled during 2003, and one of them rotated into the vertical.

The cold test of the first cryostat is scheduled for the summer of 2004, and the second cryostat should be filled by early 2005.

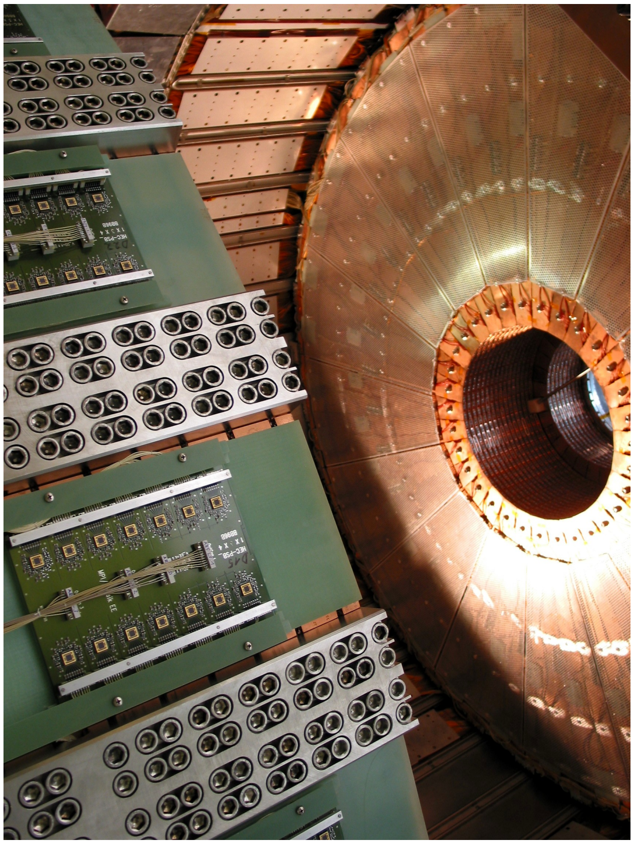

Fig. 7. The second HEC wheel being inserted into the first endcap cryostat.

The ATLAS Endcap Signal Feedthroughs

(M. Lefebvre, Victoria)

As described in detail in the 1996 Annual Report, ATLAS is building a multi-purpose *pp* detector which is designed to exploit the full discovery potential of the Large Hadron Collider (LHC) at CERN. The TRIUMF group is responsible for the engineering of the hadronic endcap calorimeter (HEC), and contributes to the production of high density cryogenic signal feedthroughs for both endcap cryostats. The feedthroughs are critical to the success of ATLAS. They have been built and tested at the University of Victoria by TRIUMF and Victoria staff. The endcap signal feedthroughs have been installed on the two endcap cryostats between December, 2002 and September, 2003. The ATLAS endcap signal feedthrough project was covered in detail in the 2001 TRIUMF Annual Report. This final endcap signal feedthrough project report focuses on the 2003 activities.

Reviews

A Canadian involvement in the endcap signal feedthroughs was already proposed in 1995. From the $12.2 M NSERC Major Installation Grant awarded to ATLAS in the 1997–98 competition, over $4 M was allocated to the endcap signal feedthrough project. The most recent status report was presented at the last NSERC ATLAS Review, held at TRIUMF on November 5, 2003.

Overview of the project

The ATLAS liquid argon calorimetry is composed of a barrel section and two endcap sections. Each endcap cryostat contains an electromagnetic calorimeter, two wheels of one HEC, and a forward calorimeter. The calorimeter signal and calibration lines are routed to the outside of each endcap cryostat via 25 feedthrough assemblies arranged approximately equally spaced in azimuth. The low voltage needed to operate the endcap hadronic calorimeter preamplifiers, which are located in the cold, are also supplied via the signal feedthroughs as well as various monitoring lines.

The design is based on gold plated conductive pins insulated and sealed by glass inserts in a stainless steel carrier. The carriers are then welded into the cold and ambient (temperature) flanges. A total of 1920 signal and calibration lines per feedthrough assembly is required in the chosen design. Figure 8 shows an overview drawing of one endcap signal feedthrough. The ambient and cold flanges are connected by a bellows to

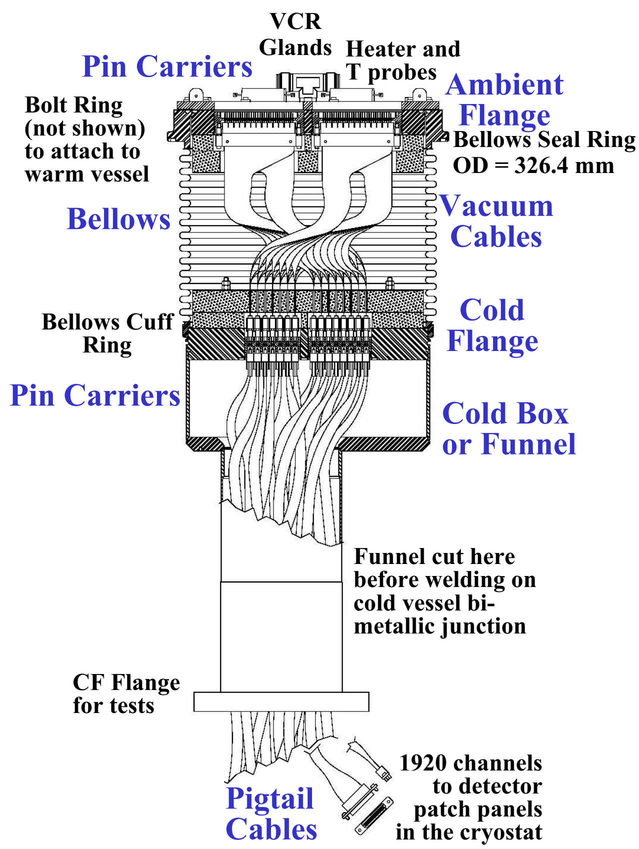

Fig. 8. Overview drawing of one endcap signal feedthrough, identifying its most important components.

isolate the feedthrough vacuum from the cryostat inter-vessel vacuum. The cold flange is attached to a transition piece, known as a funnel, which is welded to the cryostat via a bi-metallic joint. The electrical signals are brought from the calorimeter to the cold flange by coaxial kapton cables; these are called pigtail cables. Cables located in the vacuum between the cold and the ambient flange, i.e. inside the bellows, carry the signals through the cryostat wall; these are called vacuum cables. For each endcap, four feedthrough assemblies also carry the low voltage for the HEC preamplifiers.

Assembly and installation

A total of 50 feedthrough assemblies plus 5 spares has been produced following a detailed assembly procedure, quality plan and quality assurance plan. These include the description of the testing of components from their arrival in Victoria through the completion of feedthrough units. Complete material traceability is ensured through the use of detailed traveller sheets. The funnel and cold flange of each feedthrough assembly are part of the cryostat pressure vessel. An officially licensed company has done the welding and extensive testing to conform to accepted welding code.

The shipment of feedthrough assemblies to CERN was done by air freight. The last shipment was completed in January, 2003. Upon arrival at CERN, each feedthrough assembly was subjected to an ambient temperature leak test and a basic electrical test. We are responsible for these tests, the last of which were performed in June, 2003.

The installation of the feedthrough assemblies on the cryostat was a delicate and complex operation. Although the feedthrough installation is not a Canadian responsibility, our group actively assisted during the operation. The installation of the feedthrough assemblies on the first endcap cryostat started on December 2, 2002 and ended on January 4, 2003 (see Fig. 9).

Fig. 9. Paul Poffenberger (front, Victoria) during feedthrough installation on the first ATLAS endcap cryostat.

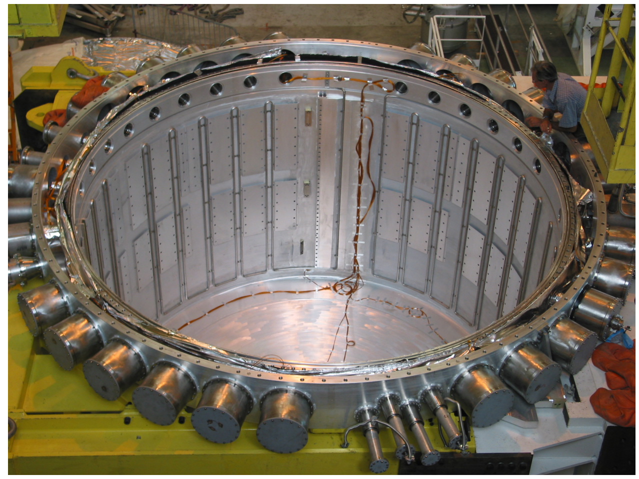

Fig. 10. Second ATLAS endcap cryostat with its cover removed, before feedthrough installation, CERN June 26, 2003.

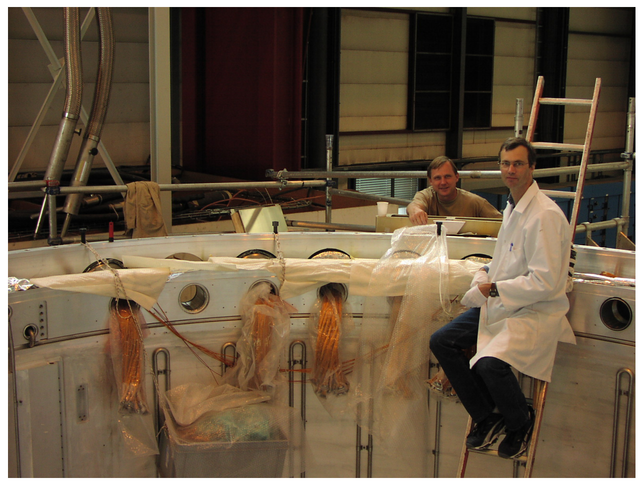

Fig. 11. Paul Birney (TRIUMF) and Ken Sexton (BNL) during feedthrough installation on the second ATLAS endcap cryostat.

Installation on the second cryostat (see Fig. 10) started on July 23, 2003 and ended on September 26, 2003 (see Fig. 11).

Members of our team manually connected the so-called warm cables that join the outside of the ambient flange to the electronics crate baseplane; each baseplane and corresponding pedestal are associated with two feedthroughs (see Fig. 12). Given the softness of the pins, this was a particularly delicate operation. Each feedthrough assembly, once welded on the cryostat, was also electrically tested (see Fig. 13). Results of these tests will form part of the ATLAS detector database.

A paper describing the ATLAS LAr signal feedthroughs is being written in collaboration with our colleagues from Brookhaven National Laboratory (who produced the barrel signal feedthroughs), and will be submitted to Review of Scientific Instruments in 2004.

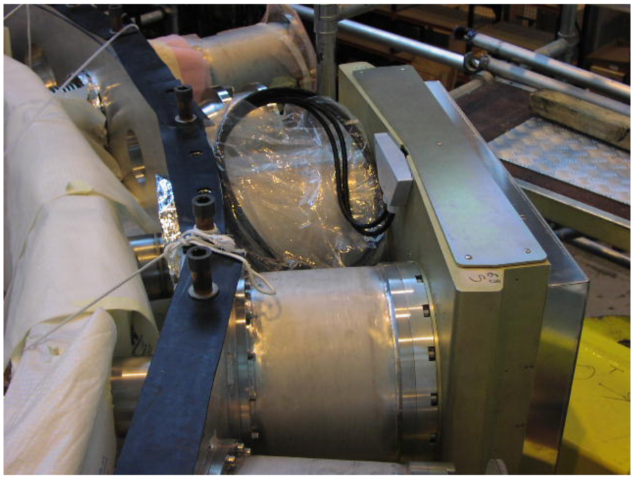

Fig. 12. View of the first mounted pedestal on the first cryostat.

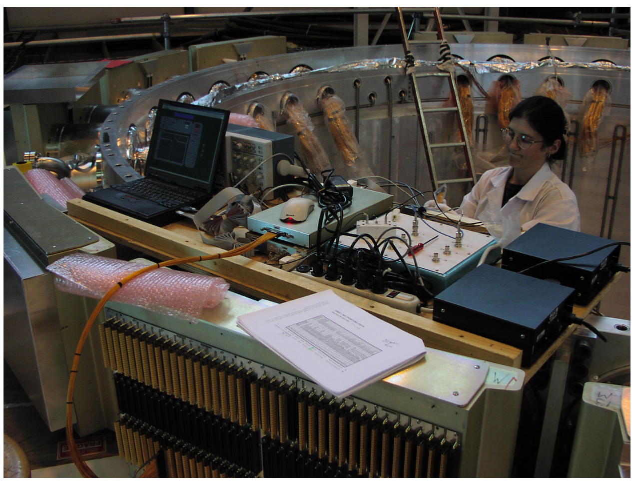

Fig. 13. Fiona Holness (Victoria) performing electrical tests on feedthroughs recently welded on an ATLAS endcap cryostat.

Other tasks in 2004 will include finalizing the inventory, the storage of spare parts, the interfacing of electrical test results with the ATLAS database, the decommissioning of the feedthrough production equipment, and the maintenance of readiness for repairs until the endcap cryostats are in operation in the ATLAS cavern.

BNL 787/949/KOPIO
Measurement of $K \rightarrow \pi\nu\bar{\nu}$ and other rare decays

(D. Bryman, UBC)

The rare kaon decays $K^+ \rightarrow \pi^+\nu\bar{\nu}$ and $K_L^0 \rightarrow \pi^0\nu\bar{\nu}$ offer unique opportunities to scrutinize higher order phenomena associated with quark mixing and charge-parity (CP) non-invariance. Experiment 787 at Brookhaven National Laboratory (BNL) discovered initial evidence for $K^+ \rightarrow \pi^+\nu\bar{\nu}$ decay based on the observation of two clean events [Adler *et al.*, Phys. Rev. Lett. **88**, 041803 (2002); *ibid.*, Phys. Rev. Lett. **84**, 3768 (2000); *ibid.*, Phys. Rev. Lett. **79**, 2204 (1997)]. The branching ratio indicated by E787 data is consistent with the standard model (SM) expectation. However, to fully explore the possibility of new physics or to make a precise measurement of the t-d quark coupling $|V_{\rm td}|$, E949 is scoped to obtain a single event sensitivity of $\mathrm{B}(K^+ \rightarrow \pi^+\nu\bar{\nu}) = (8\text{–}14) \times 10^{-12}$, roughly an order of magnitude below the SM prediction. In order to reach this sensitivity, upgrades to the E787 detector system were made and E949 commenced $K^+ \rightarrow \pi^+\nu\bar{\nu}$ data acquisition in 2002. With the completion of E949, the possibility of an inconsistency with the SM prediction of $\mathrm{B}(K^+ \rightarrow \pi^+\nu\bar{\nu})$ will be fully explored or the important top-down quark mixing parameter will be determined to a precision 15–30% if the SM expectation is confirmed.

Despite an enormous worldwide effort and significant progress in B physics, it has become evident that the K sector can yield the single most incisive measurement in the study of direct CP violation through a measurement of the branching ratio for $K_L^0 \rightarrow \pi^0\nu\bar{\nu}$ ($\mathrm{B}(K_L^0 \rightarrow \pi\nu\bar{\nu})$). In the context of the SM, $\mathrm{B}(K_L^0 \rightarrow \pi\nu\bar{\nu})$ is a unique quantity which directly measures the common area of the CKM unitarity triangles, i.e. the physical parameter that characterizes all CP violation phenomena or, alternately, the height of the triangle. Measurements of both $\mathrm{B}(K_L^0 \rightarrow \pi\nu\bar{\nu})$ and $\mathrm{B}(K^+ \rightarrow \pi^+\nu\bar{\nu})$ will allow the unitarity triangle to be precisely reconstructed from K decay information alone. Thus, a complete picture of standard model CP violation in the K system will result and a comparison with comparably precise measurements anticipated from the B sector will be enabled.

The challenges of measuring $\mathrm{B}(K_L^0 \rightarrow \pi\nu\bar{\nu})$, expected to occur at 3×10^{-11}, have been taken up by the KOPIO collaboration at BNL. KOPIO employs a low energy, time structured K_L^0 beam to allow determination of the incident kaon momentum. The goal of KOPIO is to discover the reaction $K_L^0 \rightarrow \pi^0\nu\bar{\nu}$ and obtain a sample of at least 40 events with a signal to background ratio greater than 2:1. This will yield a statistical uncertainty in the measurement of the area of the CKM unitarity triangle of less than 10%. Capital construction for KOPIO is presently planned to begin in 2005.

E787/949

The decay $K^+ \rightarrow \pi^+\nu\bar{\nu}$ had been sought since the early 1960s as an indication of the existence of flavour changing neutral currents. E949 grew out of the successful precursor experiment, E787, which took data from 1995–98 and improved the sensitivity to $K^+ \rightarrow \pi^+\nu\bar{\nu}$ by four orders of magnitude beyond previous attempts. E787 discovered the first two $K^+ \rightarrow \pi^+\nu\bar{\nu}$

events as well as several other important rare K decays and performed many non-SM searches.

The result for E787 data, based on two observed events and the expected background levels, was $B(K^+ \to \pi^+\nu\overline{\nu}) = 1.57^{+1.75}_{-0.82} \times 10^{-10}$. This result is consistent with the SM prediction. Even with low statistics, the E787 result already impacts limits on SM quark mixing and CP violation parameters, as well as possibilities for new physics as illustrated by D'Ambrosio and Isidori [hep-ph/0112135 (2002)].

Progress has also been made to access the region below the $K_{\pi 2}$ peak. Analysis of two E787 data sets (1996–97) has been completed. Combining the results, one event was found with an expected background of 2 ± 1 events giving a limit $\mathrm{B}(K^+ \to \pi^+\nu\overline{\nu}) < 2 \times 10^{-9}$ (90% CL) [Adler *et al.*, Phys. Lett. **B537**, 211 (2002)]. Since the lower region of phase space is more sensitive to new types of physics arising from scalar and tensor interactions, new limits have been derived on such couplings as well as new limits on processes like $K^+ \to \pi^+ X$. Substantial improvements will be made in E949.

E949 was based on incremental upgrades to the techniques and technology of E787. A drawing of the E787 detector upgraded for E949 is shown in Fig. 14. With the approved E949 running time of 6000 hours (about 60 weeks), the expected single event sensitivity for $K^+ \to \pi^+\nu\bar{\nu}$ is 1.7×10^{-11}. Combined with the E787 data, the sensitivity will be 1.4×10^{-11} with 0.7 expected background events. With the added acceptance from the region below the $K^+ \to \pi^+\pi^0$ peak, the sensitivity may reach 7.6×10^{-12}. We would therefore expect to see 7 to 13 events if the branching ratio is equal to the central SM value.

E949 had a short initial running period in 2002 in which approximately 2×10^{12} kaons were stopped (roughly one third of the number collected by E787). Problems with high voltage breakdown in the electromagneto-static separators forced E949 to run with a larger pion contamination and with 50% fewer kaons

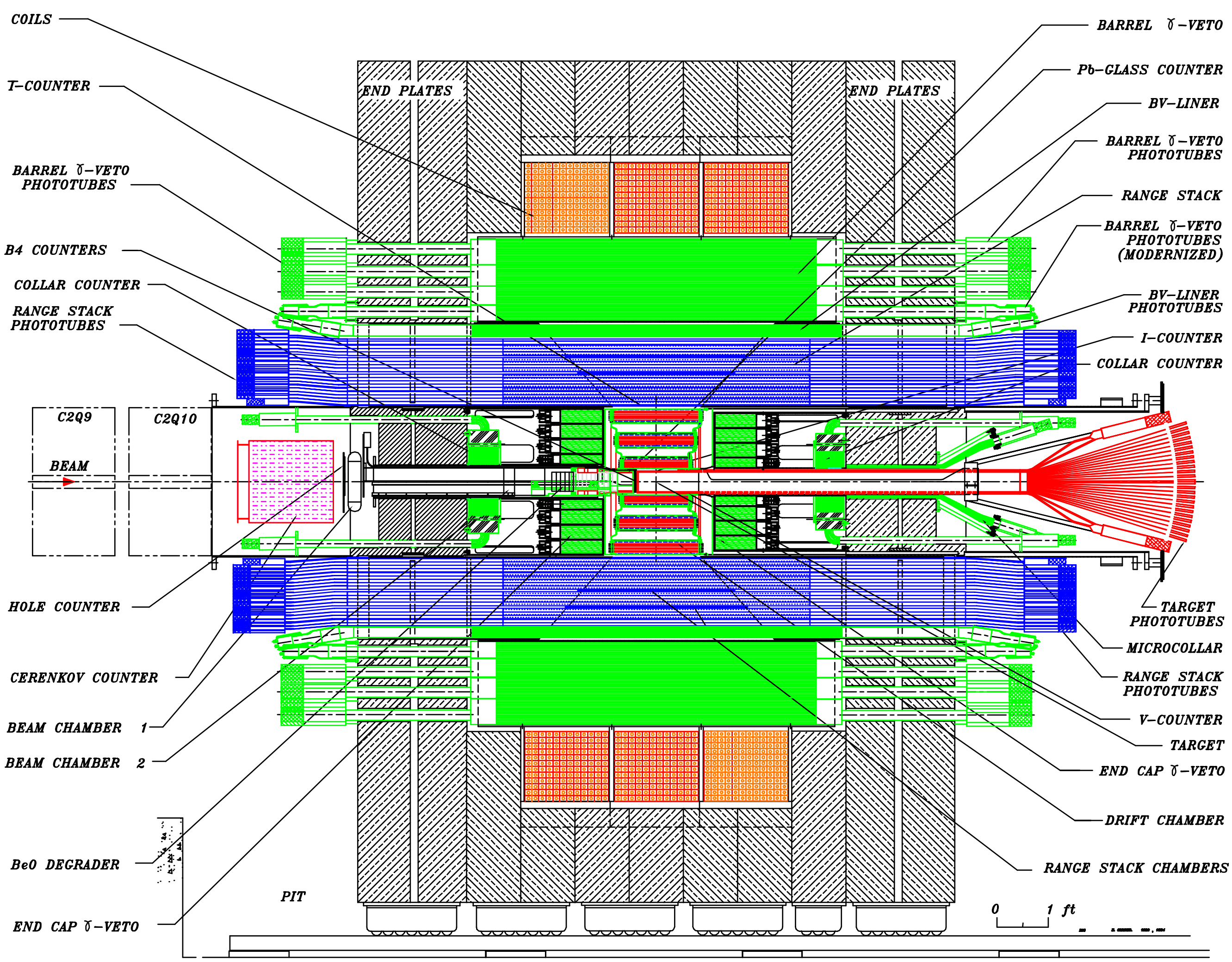

Fig. 14. The E949 detector.

per proton. The primary motor generator set for the AGS had been damaged, necessitating the use of the backup set, which required running at the reduced duty factor of 41% and with lowered primary proton beam momentum. These problems will be corrected before future running of E949.

In spite of these difficulties the projected improvements for E949 were confirmed. The analysis of the 2002 data was completed during 2003 at TRIUMF with assistance from BNL and Japan and results are expected to be published in early 2004.

KOPIO R&D

Overview The goal of KOPIO is to observe and definitively measure the rate of the decay $K_L^0 \to \pi^0 \nu \bar{\nu}$. We aim to unambiguously detect a large sample of events so that η, the SM CP violation parameter, can be determined to 15% accuracy with minimal contributions from background or systematic effects. Like E787/E949, KOPIO has built-in redundancies and a reasonable level of contingency to meet the goal of a successful measurement.

In the KOPIO experiment, a 500 μsr solid angle neutral beam is extracted at 45° to produce a "soft" K_L spectrum peaked at 0.65 GeV/c; kaons in the range from about 0.5 GeV/c to 1.3 GeV/c will be used. Downstream of the final beam collimator is a 3.5 m long decay region which is surrounded by the main detector. The decay region is surrounded by an efficient Pb/scintillator photon detector which serves to veto photons and charged particles. In the forward detection region the primary photon detector system consists of two sections: a fine grained preradiator (PR) in which the photons are converted and the first e^+/e^- pair is tracked, followed by an 18 X_0 calorimeter in which the remaining energy of the photon shower is measured. The preradiator consists of 64 0.03 X_0 layers, each with plastic scintillator, metal converter and dual-coordinate drift chambers. The preradiator, which has a total effective thickness of 2 X_0, functions to measure the photon positions and directions accurately in order to allow reconstruction of the K_L decay vertex while also contributing to the achievement of sufficient energy resolution. The calorimeter is constructed using Pb/scintillator layers. In the barrel and upstream regions, a Pb/scintillating combination will also be used to obtain high veto efficiency. Downstream of the main π^0 detector, a beam hole photon counter ("beam catcher") consists of Čerenkov detectors designed to be insensitive to neutrons.

Preradiator project The requirements of the preradiator include a photon angular resolution of approximately 25 mr, a photon conversion efficiency of about 0.7 (2.0 X_0), a good measurement of the deposited energy and as short as possible linear extent so as to limit shower size at the calorimeter. The principle employed is to measure the positions and angles of the first e^+e^- pair following photon conversion in a series of thin converter/detector modules. Each PR module consists of an inactive converter material, a dual-coordinate drift chamber (anode wires and cathode strips CSC) and a scintillator.

A stack of 5 small (8 cm × 15 cm) KOPIO chambers has been constructed and is under test. Two medium size KOPIO chambers (30 cm × 30 cm) are operational for electronics development and specification and cosmic ray measurements. Initial measurements gave the expected level of performance of full efficiency and good position resolution. The maximum drift was measured to be 70 ns with full efficiency. Position resolution was found to be $\sigma = 200$ μm for both anodes and cathodes which is more than adequate for KOPIO. Two other chambers with full scale (2 m) in one dimension (anode or cathode) are under development. The anode version was completed and is undergoing test measurements with prototype electronics. These will be used primarily for final electronics development and testing. The final prototype level will be a full size pre-production model of eight chamber layers.

Front end chamber electronics systems for both the anodes (including HV distribution) and cathodes have been tested on the development chambers. Multiple channel boards are being constructed. Designs have been developed for the receiver and processor boards at TRIUMF. Montreal has responsibility for the cathode digitizer/processor boards (which are also being spun off for other applications such as TIGRESS at TRIUMF). The anode processor board is under design at TRIUMF. An engineer at TRIUMF (paid by the US KOPIO collaboration) is dedicated to this work. Tests of the tracking and energy measurement performance in test beams at TRIUMF and BNL LEGS using pre-production electronics are planned.

During the past year, we have been working with a local company, CELCO (Surrey, BC) to develop the extruded scintillator for the KOPIO preradiator which will be read out with 1 mm dia. wavelength shifter fibre (wls). To achieve the light output, uniform hole diameters for the wls fibre, and the mechanical tolerances that are required for KOPIO, we have done several exploratory runs producing scintillator. The CELCO product has comparable light output to other commercial extruded scintillators. In addition, we have developed a new design for the preradiator's external veto detector along with assembly plans for the preradiator modules. To test the mechanical strength of the preradiator modules, we are performing finite element analysis studies of the proposed structure and a mechanical design model of a module is presently under construction. We will use the model to make stress and stability measurements which will be compared with the simulation studies.

Considerable infrastructure for the KOPIO project is being supplied by the CFI-supported LADD project. CFI approved the final budget in July and ordering of equipment has begun. This will be a boon to the design and construction of the KOPIO preradiator mechanical and electronic systems.

Beam studies Particle beam simulations for KOPIO are in progress at TRIUMF. The very short kaon bunches required are produced by extracting 0.15 ns (RMS) long proton bunches with 40 ns separation. Beams of this type, but not quality, became feasible at the AGS in 1997 with the development of a micro-bunched slow extracted beam which relies on the technique of squeezing the debunched beam through the gap between empty rf buckets that are centred near the extraction radius. The betatron tune depends on the longitudinal momentum; and chromatic extraction is effected by a 1/3-integer transverse resonance driven by sextupoles. The micro-bunches have high momenta and are preferentially extracted.

Along with new graphical and analysis software for displaying and processing the output, a computer program, LONG1D-SLEX, that combines rf manipulations and longitudinal tracking with the slow extraction transverse dynamics, was written to study the micro-bunching process. At first the program was used in support of experiments at the AGS with a 20 kV 93 MHz cavity yielding proton bunches of 0.3 ns length and 11 ns spacing. The 40 ns bunch spacing for KOPIO and the 0.15 ns bunch length at the lower frequency (25 MHz) is somewhat more challenging; a solution that makes economical use of rf voltage is required. The computer program was used to study an innovation in which a higher harmonic cavity is used to distort and stretch the rf buckets. The presently favoured scheme uses a 3 s magnet cycle, the natural chromaticity, and fundamental and anti-phased fourth harmonic cavities each with 150 kV. Currently missing from the simulations are the influence of collective effects due to wake fields.

In addition to simulating the primary beam, we have also been studying the neutral beam to insure that the beam halo of neutrons is manageable. The collimator system for the neutral beam was re-examined by studying a number of different geometries to minimize the neutron halo in the kaon decay region, especially in the vertical plane. A consensus was reached for a new geometry, which is now being used to study other aspects of the neutral kaon beam. For instance, a sweeping magnet system is being considered to sweep away charged particles in the beginning of the beam. A downstream magnet is intended to eliminate the charged kaons, produced by neutral kaons in the collimators. These studies are continuing in collaboration with colleagues at BNL and Yale.

Hypernuclear Physics with FINUDA at LNF Frascati

(A. Olin, P. Amaudruz, TRIUMF; G. Beer, Victoria)

Following the long-delayed operation of the DAFNE Phi Factory at the Laboratory for Nuclear Science (LNF) at Frascati, several milestones were recently achieved in research programs with Canadian participation. After completion of successful DEAR kaonic hydrogen X-ray measurements soon to be published, the FINUDA spectrometer was rolled into the electron-positron interaction zone shared with DEAR. The scheduled engineering test run of the FINUDA detector was begun in late fall and will be continued as a data-acquisition run until spring, 2004 if it is established that both detector and accelerator are functioning well. Some years ago, TRIUMF scientists constructed and beam-tested sixteen large low mass planar wire chambers essential to the tracking, as well as participating in the construction and installation of over 2000 straw tubes and their gas distribution system. Both these components have functioned satisfactorily, despite the long delay in the scheduled start of data acquisition. A preliminary announcement in the CERN Courier summarizes the situation at the end of 2003.

The first results from the FINUDA experiment at INFN's Frascati National Laboratory show that the detector is performing well and is in good shape for its future studies of hypernuclear physics. At the XLII International Winter Meeting on Nuclear Physics in Bormio, Italy, at the end of January, the FINUDA team presented data on the performance of the detector, as well as preliminary observations of the formation of hypernuclei and their decay spectra.

The FINUDA detector was installed at the DAFNE Phi Factory in Frascati in the spring. The experiment makes use of the low-energy negative kaons emitted in the decays of the ϕ particles created in DAFNE. The decays produce an almost monochromatic beam of K^- with an energy of about 16 MeV. These low-energy K^- can come to a stop in thin targets and interact with nuclei via a strangeness-exchange reaction, where the strangeness of the kaon is transferred to a nucleus in which a neutron (containing udd quarks) becomes a lambda particle (uds).

The use of thin targets means that the FINUDA experiment can make the most of its intrinsic momentum resolution in order to provide high-resolution measurements of hypernuclear energy levels. In addition, the apparatus is designed to detect charged and neutral particles with large angular coverage and high statistics. The experiment can also measure spectra from different targets at the same time, so reducing the number of possible systematic errors.

Once the commissioning of FINUDA was complete in October, data-taking could begin with a set of targets of different nuclei – ^{6}Li, ^{7}Li, ^{12}C, ^{27}Al and ^{51}V – that were chosen to allow a variety of simultaneous studies of the formation and decay of hypernuclei. The targets form an octagon surrounding the interaction region, where the K^- are produced in the decay of ϕ particles to K^+K^- pairs. Within the target array, thin slabs of scintillator detect the highly ionizing low-energy kaons. Hypernuclear-formation events are selected by a trigger that picks out K^+K^- pairs accompanied by a fast particle (a pion) coming from the interaction of the K^- in a target.

The data indicate a momentum resolution, $\Delta p/p$ of 1.1% full width at half maximum (FWHM), corresponding to a resolution of approximately 2.5 MeV on hypernuclear energy levels. This value should improve after final calibration and detector alignment. The indications are that during its first phase of data-taking FINUDA should collect about 3×10^5 useful events per target – which is enough for some high-resolution spectroscopy on the various nuclei. The ^{12}C spectra are already comparable in quality to the best results from KEK.

The HERMES Experiment

(C.A. Miller, S. Yen, TRIUMF; M.C. Vetterli, SFU/TRIUMF; M.G. Vincter, Alberta)

The HERMES experiment was designed to comprehensively study the spin structure of the nucleon. It has been running at the HERA electron accelerator at the DESY laboratory in Hamburg, Germany since 1995, measuring spin asymmetries for deeply inelastic electron scattering (DIS). The combination of a polarized high energy electron beam in a storage ring with undiluted polarized atomic gas targets is unique in this field, and has important experimental advantages. Furthermore, the spectrometer detecting the scattered electrons also has substantial acceptance and the capability to identify all types of hadrons produced in coincidence.

This was a pivotal year for the HERMES collaboration. A letter was submitted [Airapetian *et al.*, Phys. Rev. Lett. (in press)] reporting a key result distilled from all of the data recorded with longitudinally polarized hydrogen and deuterium targets from 1996 to 2000. This fulfills a primary original goal of the experiment – the determination of the polarizations of the quarks of various flavours (u, d, $\bar{u}$, $\bar{d}$ and s) relative to the spin direction of the nucleon, independent of any assumptions about their inter-relationship. The Canadian group played a major role in the analysis, and drafted the paper. In an important step in a new direction, the collaboration released a preliminary result constituting the first single-spin azimuthal asymmetries measured with a transversely polarized target. These data shed first light on the path towards the determination of the unknown transversity quark distribution. They are presented here, followed by one other highlight from the year's new results.

Transversity

The relativistic motion of partons inside the proton can be interpreted in a frame in which the proton is moving with "infinite" momentum, where the parton motion transverse to this direction is effectively frozen. Nucleon structure can then be investigated through measurements of parton distributions in x, the dimensionless Bjorken scaling variable representing the longitudinal momentum fraction of the proton carried by the parton. After averaging over intrinsic transverse quark momentum p_T, for each quark flavour three fundamental distributions in x can be interpreted as probability densities. Two of these have already been experimentally explored in some detail – the spin-independent density $q(x)$, and the helicity density $\Delta q(x) \equiv q^{\overrightarrow{\Rightarrow}}(x) - q^{\overleftarrow{\Rightarrow}}(x)$ reflecting the probability of finding the helicity of the quark to be the same as that of the target nucleon. Viewed in the same helicity basis, the third distribution known as transversity, δq or alternatively h_1^q, is related to a forward scattering amplitude involving helicity-flip ($N^{\rightarrow}q^{\leftarrow} \rightarrow N^{\leftarrow}q^{\rightarrow}$) and has no probabilistic interpretation. However, it is a probability density in a basis of transverse spin eigenstates: $\delta q = q^{\uparrow\Uparrow} - q^{\uparrow\Downarrow}$. The transversity and helicity densities differ only because quarks probed with sufficient spatial resolution (or sufficiently hard scattering) move relativistically, in which regime boosts and rotations don't commute.

Transversity has thus far remained unmeasured because it is chiral-odd, and hard interactions conserve chirality. However, it may be probed by a process involving some additional chiral-odd structure. If a hadron produced from the struck quark is detected in addition to the scattered lepton in semi-inclusive measurements, the distribution of the hadrons in the azimuthal angle ϕ about the virtual photon direction relative to the lepton scattering plane (see Fig. 15) can be sensitive to the transverse polarization of the struck quark. The fragmentation function $H_1^{\perp}$ describing this dependence is indeed chiral-odd, and also odd under naive time reversal (T-odd). Known as the Collins

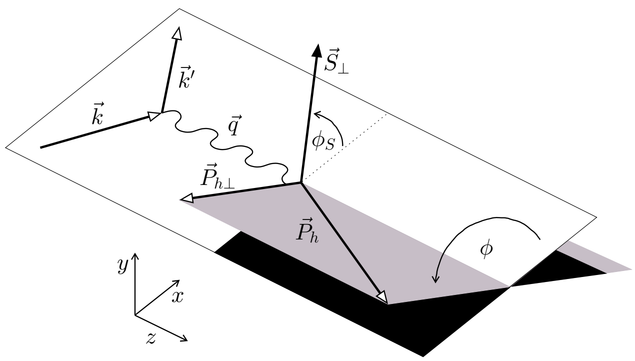

Fig. 15. The definitions of the azimuthal angles of the hadron production plane and the target spin axis.

function, it represents the interference of two amplitudes with different imaginary parts that can account for single-spin asymmetries in the ϕ distribution. Such asymmetries involving longitudinal target polarization have already been observed in pion electroproduction by HERMES. Theoretical interpretation of those data in terms of transversity-related distributions, as well as recent theoretical calculations, suggests that the Collins function has a substantial magnitude, thereby implying that measurements employing transverse target polarization can constrain transversity itself. HERMES has now released preliminary results for the first such measurements.

Azimuthal asymmetries measured with transverse target polarization can also provide another completely different window on non-perturbative QCD. It was realized over a decade ago that such asymmetries might arise from correlations between the transverse polarization of the target nucleon and the intrinsic transverse momentum of quarks. A vestige of that quark transverse momentum can survive both the photo-absorption and the ordinary fragmentation process and influence the transverse momenta of the produced hadrons, and hence their azimuthal distributions. Recently this idea has found a new reformulation "near to the heart" of non-perturbative QCD. It was realized that single-spin asymmetries that can be attributed to p_T-dependent parton distributions, such as the "Sivers function" $f_{1T}^{\perp}$ describing the correlation of p_T with target polarization, can also be understood in terms of a final-state interaction (FSI) via a soft gluon. This FSI is a model for a gauge link that is necessary to restore colour gauge invariance. A key point is that the FSI offers a mechanism to create the interference of amplitudes that is associated with the T-odd nature of the Sivers function, which was once believed to forbid its existence. A closely-related chiral-odd partner $h_1^{\perp}$ of the chiral-even Sivers function was found to provide an explanation for the substantial observed $\cos 2\phi$ dependence of unpolarized Drell-Yan cross sections. The Sivers function itself is predicted to create Drell-Yan single-spin asymmetries, but there it is predicted to have the opposite sign to its appearance in DIS, due to the fundamental time reversal symmetry of QCD. This prediction of perturbative QCD needs to be tested experimentally.

Single-spin azimuthal asymmetries arising from the Collins and Sivers mechanisms both have a $\sin\phi$ behaviour when the target is polarized along the lepton beam axis, as was the case for all previously published DIS data. However, the additional degree of freedom representing the azimuthal angle ϕ_S of the axis of transverse target polarization results in distinctive signatures – $\sin(\phi-\phi_S)$ for the Sivers mechanism, and $\sin(\phi+\phi_S)$ for the Collins mechanism. Only the Collins mechanism is sensitive to the orientation of the lepton scattering plane because it depends on the acquisition in the fragmentation process of transverse momentum k_T by the struck quark orthogonal to its transverse polarization, *after* its spin component in the lepton scattering plane has been flipped by the photo-absorption. On the other hand, the Sivers effect arises through the struck quark "remembering" the p_T that it had in the target. In either case, the struck quark transverse momentum tends to be inherited by a leading hadron that may "contain" this quark. Hence the hadron transverse momentum component $P_{h\perp}$ orthogonal to the virtual photon direction is correlated with k_T (p_T) in the case of the Collins (Sivers) effect.

In the analysis reported here, the cross section asymmetry in the target polarization is extracted as a two-dimensional distribution in ϕ versus ϕ_S, which is then fitted with a sum of contributions from the above two sinusoidal dependences. This simultaneous extraction of both the Collins and Sivers Fourier components was shown by detailed Monte Carlo simulations to avoid cross-contamination, even when they have very different magnitudes in the context of a limited detector acceptance.

The extracted Collins and Sivers asymmetries averaged over the experimental acceptance are shown in Table IV for production of π^+ and π^- mesons. The statistical precision is limited because these data were recorded in the fall of 2002 and the first two months of 2003, when the HERA beam delivery was

Table IV. Collins and Sivers virtual-photon asymmetries averaged over the experimental acceptance, which is defined in part by the ranges $0.023 < x < 0.4$ and $0.2 < z < 0.7$. The uncertainties given for each value are statistical and systematic.

	A_{C}^{h} (Collins)	A_{S}^{h} (Sivers)
π^+	$0.021 \pm 0.007 \pm 0.018$	$0.017 \pm 0.004 \pm 0.012$
π^-	$-0.038 \pm 0.008 \pm 0.022$	$0.002 \pm 0.005 \pm 0.014$

seriously hampered by backgrounds in the two collider detectors (which have since been cured). Many more data have since been recorded, and this will continue until mid-2005. The selected ranges in x and z are $0.023 < x < 0.4$ and $0.2 < z < 0.7$, and the corresponding mean values of kinematic parameters are $\langle x\rangle = 0.09, \langle y\rangle = 0.54, \langle Q^2\rangle = 2.41$ GeV^2, $\langle z\rangle = 0.36$ and $\langle P_{h\perp}\rangle = 0.41$ GeV. Here z is the fraction of the virtual photon energy carried by the detected hadron. The dependences of the asymmetries on x and z are shown in Figs. 16 and 17. No corrections were applied for the effects of instrumental smearing or acceptance, the latter of which was found to be negligible in Monte Carlo simulations.

The averaged Collins asymmetry is positive for π^+ and negative for π^-, by about three standard deviations. This can be expected if the transversity densities resemble the helicity densities to the extent that δu is positive and δd is negative and smaller in magnitude, as models predict. However, the magnitude of the π^- asymmetry appears to be at least as large as that for π^+. The left part of Fig. 16 shows that this trend becomes more apparent as the magnitudes of these transverse asymmetries increase at larger x where valence quarks tend to dominate, as did the longitudinal asymmetries previously measured by HERMES. However, the large negative π^- asymmetries might be considered unexpected as neither quark flavour dominates π^- production like the u quark dominates π^+, and one expects $|\delta d| < |\delta u|$ in analogy with $|\Delta d| < |\Delta u|$. This expectation is reflected in model predictions based on the interpretation of those longitudinal asymmetries. This failure of those predictions could be due to the neglect of the Sivers mechanism, the contribution of sea quarks or disfavoured Collins fragmentation. On the other hand, the dependence of the Collins asymmetries on z shown in the right part of Fig. 16 are not so inconsistent with theoretical predictions that they should increase with increasing z.

An interpretation of the acceptance-averaged asymmetries in the quark-parton model indicates that the disfavoured (e.g. up quark to π^-) Collins fragmentation function has the opposite sign to the favoured one (e.g. up quark to π^+), and probably has a substantial magnitude. This represents the first information about the flavour dependence of the Collins function. Work by others is now under way to extract the Collins functions from Belle e^+e^- data. This information will help to extract information about transversity from the HERMES data now being recorded.

The averaged Sivers asymmetries are significantly positive for π^+ (by four standard deviations for π^+), which constitutes the first evidence for a T-odd parton distribution function appearing in leptoproduction. The π^- Sivers asymmetries are consistent with zero. Some theoretical predictions for the Sivers function $f_{1T}^{\perp}$ have recently emerged. Since the π^+ asymmetries should be dominated by *up* quarks, the positive tendency implies a positive value for the Sivers function of this flavour, which already disfavours some theoretical models. The fragmentation function believed to combine with this quark distribution is the familiar spin-independent $D_1(z)$, which also appears in the unpolarized cross section constituting the denominator

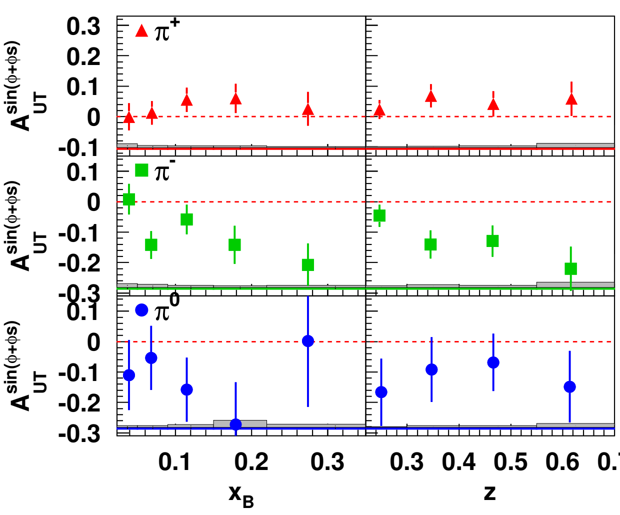

Fig. 16. Collins asymmetries for electroproduction of pions as labelled, as a function of x and z. The error bars represent the statistical uncertainties, while the lower band represents a possible interpretive uncertainty from diffractive vector meson production. In addition, there is a common overall scale uncertainty in the asymmetries that is 8% of the central value in each bin.

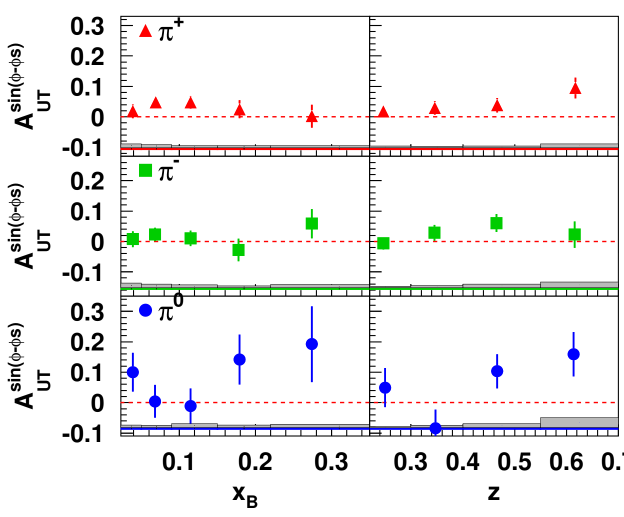

Fig. 17. Sivers asymmetries for electroproduction of pions as labelled, as a function of x and z. The uncertainties are shown as in Fig. 16.

of the asymmetry. Hence the Sivers asymmetries should depend only weakly on z, whereas the π^+ and π^0 data shown in Fig. 17 may have a surprising tendency to be more prominent at large z. The fact that the relevant fragmentation functions are known in this case implies that it will be possible to extract the Sivers distribution functions from the data now being recorded. Future Drell-Yan measurements in a polarized proton collider will be able to determine if the Sivers functions have the expected opposite sign in that process.

The pentaquark

For several years prior to 2003, the field of baryon spectroscopy had been relatively inactive. The Particle Data Group dropped their discussion on exotic baryon searches after 1988. However, starting even in the early days of QCD in the 1970's, there had been various theoretical predictions that resonances based on five-quark configurations could be narrow enough to be detectable. In 1997, calculations in the chiral quark soliton model predicted a narrow $uudd\bar{s}$ state at 1540 MeV, unbound by only 100 MeV with respect to its only strong decay channel to NK. Such a state would have "manifestly exotic" quantum numbers in the sense that its value of +1 for strangeness rules out a three-quark configuration. The first evidence for such a state appeared in 2003 as a narrow peak at 1540 ± 10(syst) MeV in the K^- missing mass spectrum for the $\gamma n \rightarrow K^+K^-n$ exclusive reaction on ^{12}C [Nakano *et al.*, Phys. Rev. Lett. **91**, 012002 (2003)]. This decay mode uniquely identifies a $S{=}{+}1$ resonance, now known as the Θ^+. Confirmation came quickly from a series of experiments, with the observation of sharp peaks in nK^+ and pK^0_S invariant mass spectra near 1540 MeV, in each case with a width limited by the experimental resolution. Taken together, these results, all based on data previously recorded for other purposes, were heralded as the discovery of the first manifestly exotic hadron in the 40 years since the Ω^-.

HERMES made significant contributions to this set of data. Further evidence for the pentaquark resonance was detected as a peak in the proton-K^0_s invariant mass spectrum in quasi-real photoproduction on deuterium. The good mass resolution of the HERMES spectrometer with well-understood systematics provided more restrictive information related to the mass and isospin of the resonance than did previous publications. Figure 18 shows the pK^0_s mass spectrum, compared with a fit based on a model for the background that incorporates a simulation of the non-resonant background together with fitted peaks for known Σ^{+*} resonances. The mass of 1528 ± 2.6(stat)± 2.1(syst) MeV resulting

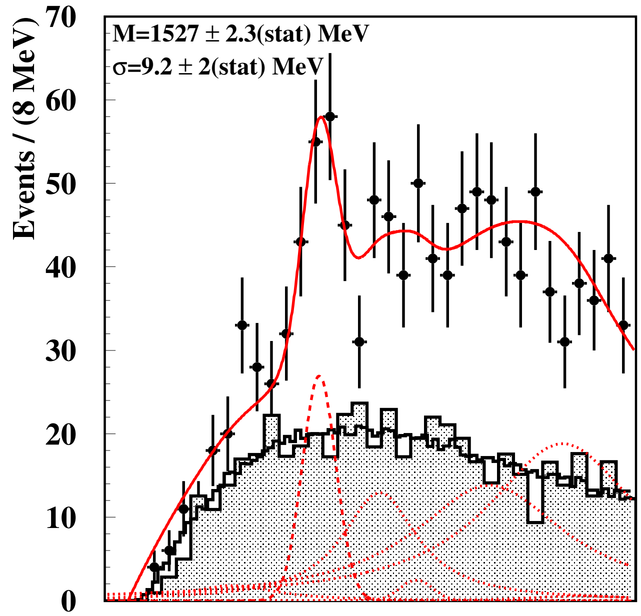

Fig. 18. Distribution in invariant mass of the $p\pi^+\pi^-$ system. The experimental data are represented by the filled circles with statistical error bars, while the fitted smooth curves result in the indicated position and σ width of the peak of interest. A PYTHIA6 Monte Carlo simulation is represented by the gray shaded histogram, a mixed-event background model normalized to the PYTHIA6 simulation is represented by the fine-binned histogram, and the fitted curve includes in addition a Gaussian fitted to the peak of interest and Breit-Wigner peaks with the positions and widths of various known Σ^{*+} resonances but with free amplitudes.

from the fit was the most precise value at the time, and constituted a departure from the earlier reports, which had clustered around 1540 MeV. However, mass values subsequently reported by other experiments have also tended to fall below 1530 MeV. Another contribution was the first indication of a finite width of the resonance after accounting for instrumental resolution. The ZEUS Collaboration has since also reported such an indication.

There has been theoretical speculation that the small width of the Θ could be understood if it were a member of an isospin multiplet, whose decay violated isospin conservation. HERMES contributed strong evidence that the Θ^+ is an isosinglet. Figure 19 shows distributions in $pK^{\pm}$ invariant mass. While the $\Lambda(1520)$ appears where expected in the pK^- spectrum, the pK^+ spectrum shows no sign of a Θ^{++}, in spite of the acceptance being about 30 times larger for this decay than for pK^0_s.

The ongoing HERMES program

DESY has promised beam for HERMES until at least the end of 2006, probably until mid-2007. The present HERMES running plan is to continue until mid-2005 on the transversely-polarized hydrogen

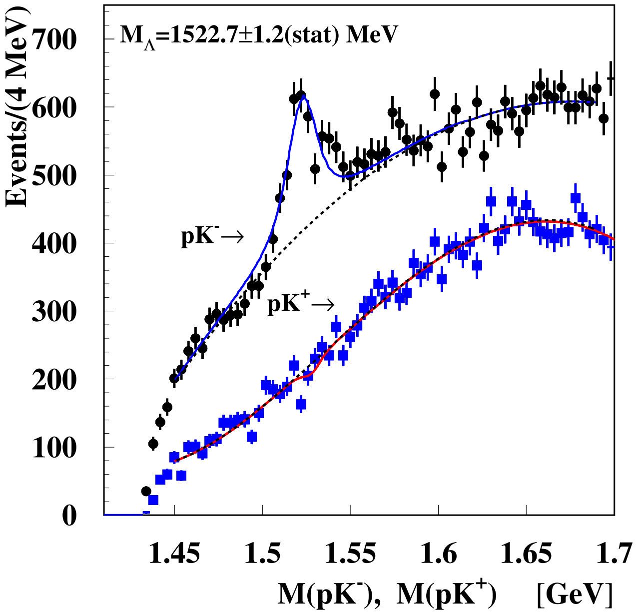

Fig. 19. Spectra of invariant mass M_{pK^-} (top) and M_{pK^+} (bottom). A clear peak is seen for the $\Lambda(1520)$ in the M_{pK^-} invariant mass distribution. However, no peak structure is seen for the hypothetical Θ^{++} in the M_{pK^+} invariant mass distribution near 1.53 GeV.

target to complete the first measurement of quark transversity in the proton. Meanwhile, HERMES is assembling a new recoil detector to surround the target cell and detect the recoiling intact target nucleon from hard exclusive processes, in order to guarantee their exclusivity. This fully funded €1.4 M project is scheduled to be ready for two years of running on high density unpolarized targets in 2005/7. This will yield the first really high quality data on asymmetries in both beam spin and charge for DVCS, the process that holds the most promise to shed light on the orbital angular momentum of partons.

HERMES collaborators in 2003: G. Gavrilov, J. Lu, C.A. Miller, S. Yen (TRIUMF); M.V. Vetterli (SFU/TRIUMF); M.G. Vincter (Alberta); K. Garrow (Alberta/SFU); J. Wendland (SFU).

J-PARC
T2K long baseline neutrino experiment

(A. Konaka, TRIUMF)

Introduction

Convincing evidence for neutrino oscillations has recently been obtained in measurements of both solar and atmospheric neutrino interactions by the Super-Kamiokande and SNO collaborations. The KamLAND experiment independently confirmed the solar neutrino oscillation effect using reactor neutrinos. It determined the mass difference Δm^2_{12} and the mixing angle θ_{12} to be consistent with the large mixing angle (LMA) solution. The K2K experiment observed oscillations of accelerator-produced muon neutrinos, in agreement with the observation of oscillation of atmospheric muon neutrinos at the 99% confidence level using neutrinos from an accelerator beam at KEK. K2K has started to see an indication of the energy dependence of the oscillations.

The next step is an accelerator-based long baseline experiment to determine the remaining parameters of the lepton mixing matrix: the first to third generation mixing angle θ_{13} and the CP-violating phase, δ_{CP}. The most promising avenue for measuring these parameters is to study $\nu_\mu \rightarrow \nu_e$ oscillations using so-called "superbeams" – high intensity neutrino beams derived from the decays of pions. The large statistics provided by a superbeam will also greatly improve the precision with which the mixing parameters Δm^2_{23} and θ_{23} can be measured. A number of initiatives are being considered worldwide to address this physics. The most advanced program is the J-PARC (Japan Proton Accelerator Research Complex) to Super-Kamiokande (SK) experiment (see Fig. 20). This neutrino project, which is called T2K (Tokai to Kamioka), submitted a letter of intent (LOI) signed by 155 physicists from 12 countries to the J-PARC office in January, 2003. Twenty scientists from Canada signed this LOI. J-PARC has been under construction since April, 2001. Funding for the neutrino beam line was approved by the Japanese government in December, 2003, and the first T2K international collaboration meeting will be held in January, 2004. An NSERC grant for an R&D of T2K near detector has been awarded to the Canadian T2K collaboration (TRIUMF, UBC, UVic, Alberta, Toronto and York).

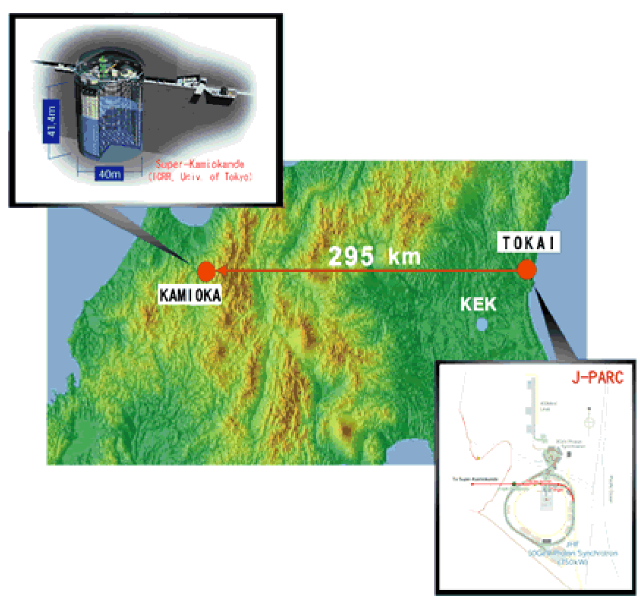

Fig. 20. A neutrino beam produced at J-PARC will be sent to the Super-Kamiokande detector located 295 km away.

Canadians have been involved from the beginning of the T2K project and have made a number of important contributions to the physics, including the off-axis concept, the ν_e appearance analysis, and a study of the prospects for measuring CP violation. Canadians have also made important contributions to the accelerator design, including studies of the beam transport using combined function superconducting magnets and a dual abort/extraction kicker concept. A JHF(J-PARC) neutrino workshop was held in February when eight J-PARC facility construction members visited TRIUMF. An R&D collaboration between TRIUMF and KEK on the J-PARC project was discussed. Contributions to J-PARC's accelerator and neutrino beam line components are proposed for the next TRIUMF 5 year plan. In June, some of the Canadian T2K members joined the K2K experiment, which is an ongoing long baseline neutrino experiment from KEK to Super-Kamiokande. K2K is an ideal prototype experiment for the T2K project, providing a test bed in which to develop equipment and methods that will later be adapted to T2K.

The T2K project

Overview The J-PARC accelerator is a 50 GeV proton synchrotron currently under construction, and will begin operation in 2008. It will be the first MW class machine (0.75 MW) in this energy range. The construction of the neutrino beam line was funded by the Japanese government in December, and the beam line commissioning is expected in January, 2009. The far detector already exists, namely the well-understood 50 kton water Čerenkov Super-Kamiokande (SK) detector. The experiment uses a narrow-band neutrino beam whose energy is tuned to the oscillation maximum (0.5–1.0 GeV) given the distance from J-PARC to SK (295 km). The technique which has been adopted is to aim the neutrino beam 2–3° away from the detector (off-axis beam). This idea was originated by a Canadian group in connection with BNL proposal E889. This method provides a larger ν_μ flux and a smaller ν_e contamination than other methods for producing narrow-band beams. The neutrino energy will be reconstructed through the two body quasi-elastic (QE) scattering reaction, $\nu n \to l^- p$. The T2K neutrino energy of 0.5–1.0 GeV is ideal, because the cross section is dominated by the QE scattering. A new fine-grained detector of several tonnes will be placed 280 m from the production target to provide measurements of the neutrino beam flux.

Precision measurement of the oscillation pattern The oscillation pattern of the ν_μ disappearance is measured precisely as a function of the reconstructed neutrino energy.

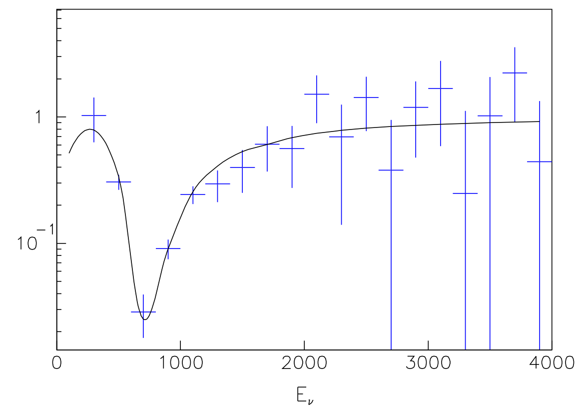

Fig. 21. The ratio of the measured neutrino energy spectrum to the expected one without neutrino oscillation, as a function of neutrino energy in MeV, after subtracting non-QE events.

Figure 21 shows the ratio of the measured neutrino energy spectrum to the expected one without neutrino oscillation. The position and the depth of the dip in this ratio provide Δm^2_{23} and $\sin^2 2\theta_{23}$, respectively. The goal of the experiment is to achieve an order of magnitude improvement in precision of the ν_μ disappearance parameters: $\delta(\Delta m^2_{23}) \sim 0.01$ and $\delta(\sin^2 2\theta_{23}) \sim 1 \times 10^{-4}$ eV^2. Deviation of the pattern from the neutrino oscillation prediction would indicate new physics beyond the MNS matrix, such as sterile neutrinos, extra dimensions, or new leptonic flavour changing neutral current interactions. Comparison of Δm^2_{23} and $\sin^2 2\theta_{23}$ between ν_μ and $\bar{\nu}_\mu$ provides a precise test of CPT conservation in neutrino oscillation. The neutral current to charged current ratio (NC/CC), similar to what is studied by SNO for the solar ν_e disappearance, provides a sensitive test of the sterile neutrinos hypothesis.

$\nu_\mu \to \nu_e$ appearance: θ_{13} The $\nu_\mu \to \nu_e$ appearance channel is sensitive to the first to third generation lepton mixing angle θ_{13}. Figure 22 shows the

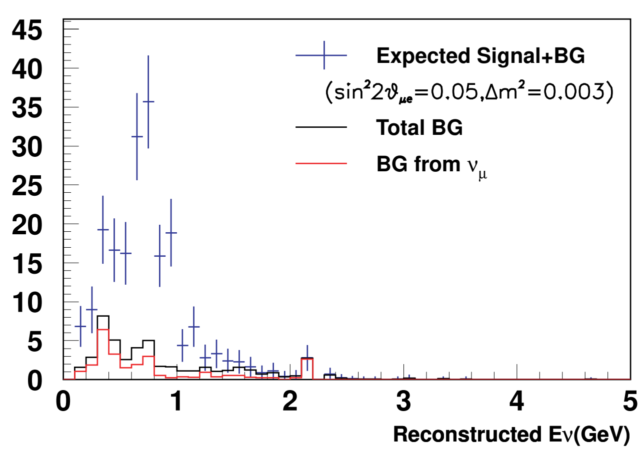

Fig. 22. Reconstructed electron neutrino energy distributions for 5 years' exposure assuming θ_{13} is at the current reactor (CHOOZ) limit.

reconstructed electron neutrino energy spectrum assuming θ_{13} is at the current reactor (CHOOZ) limit. A clean reconstructed ν_e energy peak is expected at the oscillation maximum. If θ_{13} is small, a 90% C.L. upper limit of $\sin^2 2\theta_{13} = 0.006$ ($\sin^2 2\theta_{\mu e} = 0.003$) can be achieved, which is a factor of 20 improvement over the reactor limit.

Accelerator and beam line contributions to J-PARC

High-intensity proton accelerators have long been the dream of many accelerator and particle physicists and are attracting renewed interest as sources of neutrino super-beams. A megawatt class accelerator like J-PARC will have to overcome new problems in handling unprecedented beam power. Expected Canadian contributions target the elements that are the most critical in controlling beam losses, namely the beam dynamics and damper system in the main ring, the extraction kicker magnet, beam diagnostic systems in the proton transport line, and the shielding and remote handling of the target station. All of these are areas where TRIUMF has world-leading expertise.

Detector R&D for the T2K project

There are three sets of detectors in T2K: the muon monitor in the beam dump, the fine-grained calorimeter at the 280 m near site, and the Super-Kamiokande water Čerenkov detector at the 295 km far site. The Canadian group is interested in the 280 m fine-grained calorimeter, optical calibration for the water Čerenkov detectors, and diamond sensors for the muon monitor.

Fine-grained calorimeter A fine-grained calorimeter is the optimum near (280 m) detector for T2K because the ability to measure the energies and directions of both the outgoing muon and the recoil proton will give a strong kinematic selection on the quasi-free scattering process that will dominate the cross section at the ∼700 MeV neutrino energy of this experiment, and allow the reconstruction of the incident neutrino energy and direction. This near detector is key to understanding the systematic uncertainty in the θ_{13} and θ_{23} measurements through detailed understanding of the neutrino flux and interactions at intermediate energies. Since there is a lack of data about neutrino interactions in the 1 GeV region, it provides interesting physics by itself. It also provides important information about backgrounds to the proton decay search, which will be performed concurrently by the far detector. The technology we have been studying is based on a water-soluble scintillator which is read out by wavelength-shifting fibres and photosensors. Photomultipliers, avalanche photodiodes, and silicon photomultipliers are being examined as photosensor candidates.

Strawman Manipulator Design

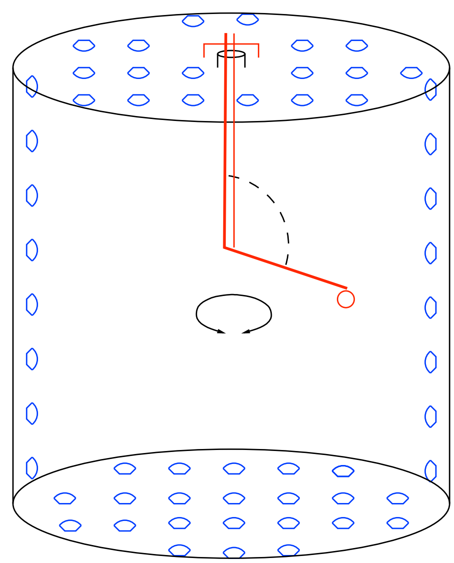

Name “Canadarm” already taken ... Calibarm???

Fig. 23. A schematic view of a deployable manipulator arm for optical calibration of the K2K near water Čerenkov detector.

Optical calibration of the water Čerenkov detectors Optical calibrations play a critical role in the T2K experiment. The systematic uncertainty on the rejection of the main π^0 background in the $\nu_\mu \to \nu_e$ appearance is determined by the knowledge of the optical properties of the water Čerenkov detector. The main systematic uncertainty in the ν_μ disappearance mode comes from the fiducial volume and the energy scale, in which optical calibrations again play the main role. Sophisticated optical calibration tools, namely an isotropic laser ball, manipulator system, and analysis procedure, have been developed by the SNO collaboration. The Canadian group participates in the K2K 1 kton water Čerenkov group and is designing a manipulator system for its optical calibration (Fig. 23).

Diamond sensors for the muon monitor Muons in the beam dump provide spill-by-spill information about the hadronic beam. In order to separate muons from hadronic showers in the beam dump, it is proposed to detect delayed Michel electrons from stopped muons decaying in the beam dump. Diamond sensors are of particular interest because of their radiation hardness and fast response, enabling the detection of Michel electrons. They may also be useful for monitoring the beam halo in the primary beam line. A diamond sensor has been installed behind the K2K beam dump in the fall, and a clear muon signal has been observed (Fig. 24).

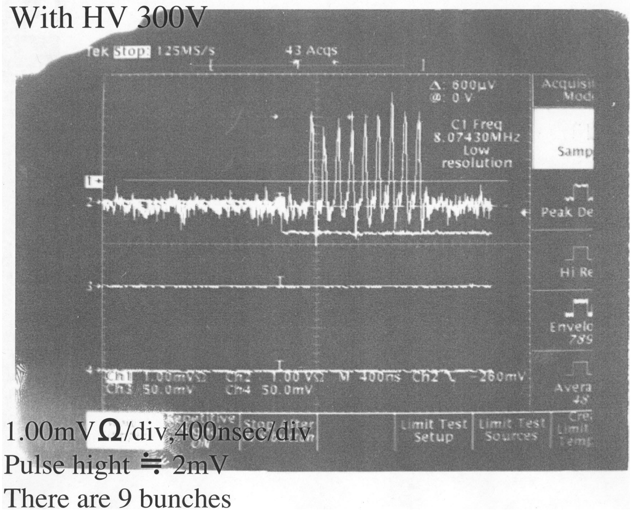

Fig. 24. Diamond signal observed behind the K2K beam dump. The 9 micro-bunch structure of the beam spill is clearly observed.

Sudbury Neutrino Observatory
(R. Helmer, TRIUMF)

Data-taking in the salt phase of SNO was completed in the past year. During this phase, detection of neutral current (NC) interactions was enhanced by the addition of 2 tons of salt (sodium chloride) to the heavy water. Neutrons from the break-up of the deuterons were detected by observing the gamma cascade following neutron capture on chlorine. The Q-value for capture on chlorine is higher than for capture on deuterium; hence there is better energy separation between these signals and those from the competing charged current (CC) reaction. The gamma cascade also implies that signals from capture on chlorine will be more isotropic than for either capture on deuterium or charged current interactions; the latter two both have only a single associated gamma. It was possible to take advantage of the isotropy to extract the neutral current interaction rate independently of assumptions about the shape of the energy spectrum.

Results based on the first 254.2 live days of data have been submitted for publication [Ahmed *et al.* (SNO collaboration), submitted to Phys. Rev. Lett., nucl-ex/0309004]. Only the distributions of isotropy, cosine of the event direction relative to the vector from the sun, and radius within the detector (to limit backgrounds) were used to extract the total numbers of CC, elastic scattering (ES), NC, and external-source neutron events. The equivalent ^{8}B fluxes for the CC, ES and NC reactions were found to be (in units of $10^6\mathrm{cm}^{-2}\mathrm{s}^{-1}$):

$$\phi_{\mathrm{CC}}^{\mathrm{SNO}} = 1.59^{+0.08}_{-0.07}(\mathrm{stat})^{+0.06}_{-0.08}(\mathrm{syst})$$

$$\phi_{\mathrm{ES}}^{\mathrm{SNO}} = 2.21^{+0.31}_{-0.26}(\mathrm{stat}) \pm 0.10(\mathrm{syst})$$

$$\phi_{\mathrm{NC}}^{\mathrm{SNO}} = 5.21 \pm 0.27(\mathrm{stat}) \pm 0.38(\mathrm{syst})\,.$$

$\phi_{\mathrm{NC}}^{\mathrm{SNO}}$ gives the total flux of active neutrinos and is consistent with solar model calculations.

These results were combined with day and night energy spectra obtained during the pure heavy water phase of the experiment, and results from other solar neutrino experiments and KamLAND, to place constraints on allowed neutrino mixing parameters. The best fit point occurs for $\delta m^2 = 7.1^{+1.0}_{-0.3} \times 10^{-5}\mathrm{eV}^2$ and $\theta = 32.5^{+1.7}_{-1.6}$ degrees. The new SNO result has further restricted the allowed LMA region and disfavours maximal mixing by 5.4 σ.

With the completion of the salt phase, SNO has entered the third, and final, phase of the experiment. Discrete ^{3}He proportional counters have been placed in the heavy water volume to provide a third, independent measurement of the neutral current interaction. Insertion of these detectors required removal of the glove box originally supplied by TRIUMF (see TRIUMF Annual Report, 1996) to aid in the deployment of calibration sources. To increase the utility of the box, one new side with extra access ports was designed and fabricated at TRIUMF. The original side was removed and the new side welded on using local shops in Kingston.

TJNAF Experiment 00-006
Measurement of the flavour singlet form factors of the proton ($G\emptyset$)
(W.T.H. van Oers, Manitoba)

The detailed structure of the nucleon at low energies is not well understood within the framework of quark and gluon degrees of freedom. For example, relatively little is known about the importance of the sea quarks at these energies. The $G\emptyset$ experiment will measure two proton ground state matrix elements which are sensitive to point-like strange quarks and hence to the quark-antiquark sea in the proton. The matrix elements of interest are the elastic scattering vector weak neutral current charge and magnetic form factors, G_E^Z and G_M^Z, respectively. These can be extracted from a set of parity-violating electron-proton scattering measurements. If one assumes a relationship between the proton and neutron structure in that the proton and neutron differ only by the interchange of up and down quarks, i.e. isospin symmetry, the strange quark (as well as the up and down quark) contribution to the charge and magnetic form factors of the nucleon can be determined. This would result from taking appropriate linear combinations of the weak neutral form factors and their electromagnetic counterparts.

Determinations of both the charge and magnetic strange quark form factors are of fundamental interest, as these would constitute the first direct evidence of the quark sea in low energy observables. It is the objective of the $G\emptyset$ experiment to determine these contributions to the proton form factors at the few per cent level. Observations at high energy suggest that the strange quarks carry about half as much momentum as the up and down quarks in the sea. It is important to determine both the role of the quark sea and the relevance of strange quarks at low energy where there are voids in understanding the theory of the strong interaction (quantum chromodynamics, QCD). Even if the strange quark contributions do not amount to the level of sensitivity of the experiment, upper limit determinations at this level are as valuable as non-zero results. The matrix elements, G_E^Z and G_M^Z, are also relevant to discussions of the Ellis-Jaffe sum rule and the pion-nucleon sigma term; there is uncertainty in both of these about the strange quark contributions. The $G\emptyset$ experiment will allow the determination of the strange contributions to the proton charge and magnetic form factors in a much more straightforward manner than is possible with regard to the corresponding observables in the above two deduced relations.

In the $G\emptyset$ experiment, which is being carried out in Hall C at the Thomas Jefferson National Accelerator Facility (TJNAF), parity-violating longitudinal analyzing powers will be measured in electron-proton scattering in the range $0.1 \leq Q^2 \leq 1.0$ GeV^2 at both forward and backward angles. The longitudinal analyzing power is defined as

$$A_z = (1/P)\frac{[\sigma^+(\theta) - \sigma^-(\theta)]}{[\sigma^+(\theta) + \sigma^-(\theta)]}$$

where P is the polarization of the incident electron beam and the + and − signs indicate the helicity state. Making pairs of measurements at forward and backward angles will allow the separation of G_E^Z and G_M^Z. Predicted longitudinal analyzing powers range from about (–3 to 35) $\times 10^{-6}$; the goal is to measure the longitudinal analyzing powers with statistical uncertainties of $\Delta A/A = 5\%$ and systematic uncertainties related to helicity correlated effects of $\Delta A/A \leq 2.5 \times 10^{-7}$.

The heart of the $G\emptyset$ detection system is a spectrometer which consists of an eight-sector toroidal magnet, with an array of scintillation detectors located at the focal surface of each octant and, for the backward angle mode, arrays of scintillation and Čerenkov detectors located near the magnet cryostat-exit window of each octant. In the first phase of the experiment, longitudinal analyzing powers will be measured concurrently at several values of the momentum transfer in the range $0.1 \leq Q^2 \leq 1.0$ GeV^2. It must be realized that the length of the experiment is in part governed by making rather elaborate control measurements to determine the corrections that have to be made to the measured asymmetries and to assess systematic errors. In the second phase of the experiment each subsequent backward angle analyzing power measurement would require from one half to one month of running time. The results of the SAMPLE experiment at the MIT-Bates Laboratory have shown the importance of measuring the axial form factor corrections, since these may be quite different from the theoretical predictions. Therefore, companion measurements of quasi-elastic scattering from deuterium will also be made at the backward angles. With these measurements, the effective axial current of the nucleon will also be determined. This current includes effects from the effective axial coupling of the photon to the nucleon or anapole moment, which are relevant also in other processes, e.g. parity violating Moller scattering and atomic parity violation.

The $G\emptyset$ collaboration

The $G\emptyset$ experiment is being carried out in Hall C at TJNAF by a collaboration of scientists from Canada, France, Georgia, and the United States, with funding provided through NSERC (Canada), IN2P3 (France), and DOE/NSF (US).

Following the completion of many critical milestones, this past year also saw the completion of a very successful commissioning run for the first phase forward angle mode of the $G\emptyset$ experiment. Preliminary analysis of the data taken under much less than ideal conditions for the experiment exhibits great promise. Considerable progress has also been made in the design, prototyping, and fabrication of critical components for the second phase backward angle mode of the experiment, in particular with the cryostat exit detectors, the aerogel Čerenkov detectors, and the support structure for these. The Canadian contributions to these efforts have been significant. Below follows an enumeration of the various Canadian contributions to the $G\emptyset$ experiment. The three components mentioned above as well as other aspects of the $G\emptyset$ experiment are described in some detail below.

Canadian contributions

The Canadian members of the $G\emptyset$ collaboration, based at the Universities of Manitoba, Northern British Columbia, and TRIUMF, have been asked to:

(1) Develop and produce specialized photomultiplier tube bases for the focal plane detector arrays;
(2) Design, build, and commission an automated magnetic field measuring (magnetic verification) apparatus complete with its own data acquisition system;
(3) Prototype and fabricate the cryostat exit detector arrays for the backward angle measurements;

(4) Prototype and fabricate (together with the Grenoble group) the aerogel Čerenkov arrays for background rejection in the backward angle measurements;
(5) Design the support structure for the aerogel Čerenkov and cryostat exit detector arrays;
(6) Coordinate the implementation of TJNAF built beam monitors and control apparatus with TRIUMF built parity electronics.

Much progress has been made in the design and construction of the various subsystems listed above, many of which are now already in operation.

Photomultiplier tube bases and magnetic verification system

The photomultiplier tube bases and magnetic verification system have been described in some detail in last year's Annual Report. Both of these construction projects have been successfully completed and the hardware is currently in operation or has already been successfully operated.

Cryostat exit detectors

For the backward angle second phase of the $G\emptyset$ experiment, the addition of a second array of scintillation detectors, located near the spectrometer cryostat exit windows, will be required in order to separate the elastic and inelastically scattered electrons. The geometry of these cryostat exit detector (CED) arrays (see Fig. 25) has been studied in detail and a reference design was completed. With the resident expertise at TRIUMF in producing high quality scintillation detectors and lightguides, the Canadian subgroup was asked to play the lead role in the prototyping and production of the CEDs. A set of prototype CEDs was built at TRIUMF and delivered to the $G\emptyset$ collaboration for studies with cosmic rays. Results from these studies showed that the reference design and the prototype detectors met the specification requirements for these arrays. Production of a full set of dummy CED prototypes was then completed at TRIUMF, to aid in the design of the CED support structure. After finalizing the CED design, construction of the production versions of the CED arrays took place in 2001. Fabrication of the CED scintillators for all 8 octants was completed and delivery made to TJNAF, and fabrication of the special helical-bent lightguides began in 2002. In order to achieve the unique helical bend required in the $G\emptyset$ back angle geometry, customized bending jigs were designed and constructed at TRIUMF and tested on a first set of prototype CED lightguides. Production of a full set of lightguides for the first CED octant was completed and delivery made to TJNAF in 2003, where they are undergoing further tests. Production of the remaining lightguides is nearing completion and they will be delivered to TJNAF in early 2004. The CEDs will also make use of the same types of photomultiplier tubes and specialized TRIUMF/$G\emptyset$ bases as the focal plane detectors.

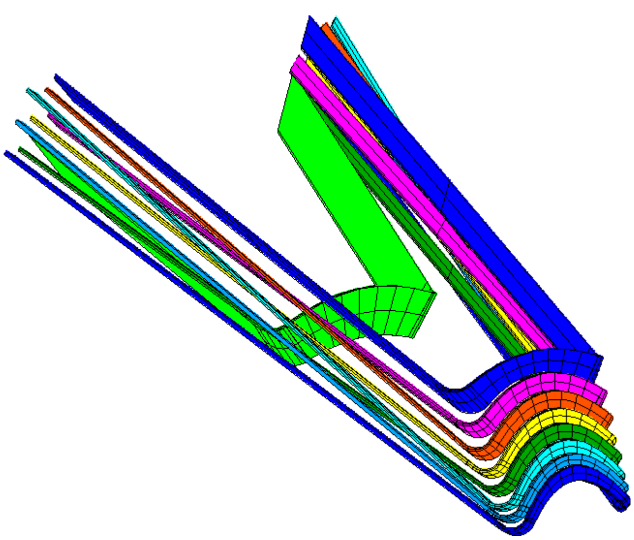

Fig. 25. Layout of a cryostat exit detector (CED) array for a single octant.

Aerogel Čerenkov detectors

Monte Carlo simulation results have shown that backgrounds from negative pions will be problematic for the second phase backward angle measurements involving the deuterium target. The $G\emptyset$ simulation subgroup has focused on characterizing this π^- background and providing options regarding the design of an additional set of detectors to reject the background pions. The $G\emptyset$ Canadian and French (Grenoble) subgroups have been asked to jointly undertake the prototyping and construction of this crucial set of detectors, which will be made up of an array of aerogel Čerenkov counters. Much effort has gone into the design of this detector array and a conceptual design (see Fig. 26) was evolved into a first prototype at TRIUMF.

Prototype tests using the TRIUMF pion beam (M11) were carried out in December, 2001, but were hampered by the fact that there was insufficient aerogel to fully load the detector, which led to inconclusive results. This situation was rectified in early 2002 (with the loan of some sample aerogel from Caltech), and further tests using cosmic rays were carried out at TRIUMF over the spring and summer of 2002. Issues that have been studied include: the optimal choice and configuration of reflective material within the light diffusion box; the choice of photomultiplier tube (PMT) and base; the best procedure to establish a hit (summed signal vs. multiplicity); characterization

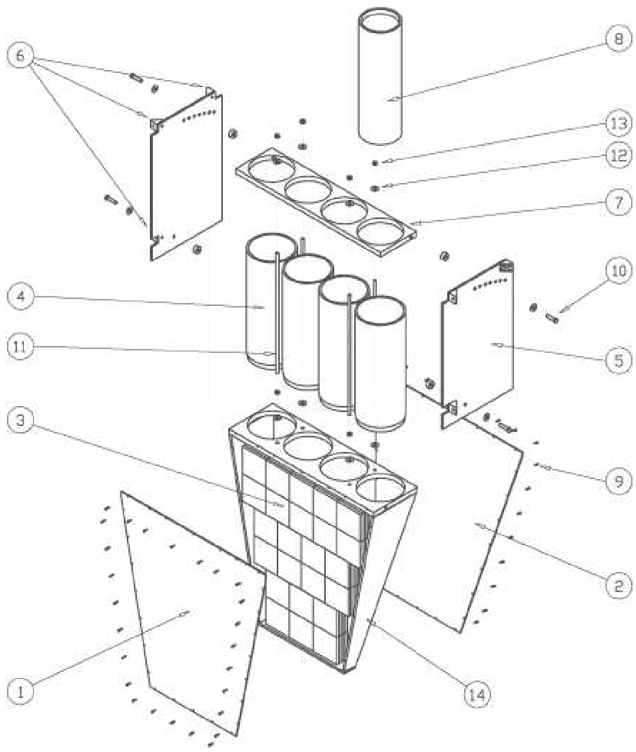

Fig. 26. Conceptual layout of the aerogel Čerenkov detector.

of the diffusion box response by Monte Carlo simulations; magnetic shield requirements; radiation shielding requirements; and optimization of the solid angle of the detector.

In the tests with cosmic rays, different PMTs were examined in the detector box and the Photonis XP4572B was chosen. Millipore paper was chosen as the diffuse reflector in the box. Most of the inner surfaces of the box were lined initially with an underlayer of Tyvek and one layer of millipore. Later, a second layer of millipore was added. The collars around the PMTs were also lined with millipore. Another issue, related to the inactive region of the photocathode around the PMT front face, was studied in detail. A reflective cone was designed to cover this region and to redirect the light toward the active portion of the PMT photocathode. Different reflective materials on this cone were tested, including an experimental reflective (dichroic) film from 3M. Although results with the dichroic reflector were initially encouraging, it was later demonstrated that good quality (thicker) aluminized mylar resulted in comparable or even slightly better detector efficiencies. Measurements were made at different positions: (i) near the PMTs, (ii) at the centre of the box, and (iii) far from the PMTs. Studies of light propagation in the diffusion box were also carried out using the programs LITRANI, GEANT4, and a simple Monte Carlo.

During this past year, tests with the prototype Čerenkov detector were carried out using both cosmic rays and the M9 and M11 beam lines at TRIUMF. With our last funding increment, we were finally able to purchase the full amount of aerogel needed to fully implement the four Canadian octants of the Čerenkov counter array. Most of this aerogel is now at Jefferson Lab, but a sufficient amount was received at TRIUMF to allow us to extend our tests. Over the summer, the sample aerogel in our prototype detector was replaced with the production aerogel, and the photon yield (and, thus, the detector efficiencies) immediately improved. Average yields of approximately 6.5 photoelectrons were observed for measurements made at the centre of the diffusion box. (With the earlier sample aerogel, which had many cracks, the average yield was closer to 5 photoelectrons, at the centre of the box.) Further tests using the TRIUMF secondary beams in M11 were carried out in late summer. After some initial problems related to magnetic shielding were resolved, very encouraging results were obtained using the electron and muon beams. Average yields of approximately 12, 8, and 6 photoelectrons were observed for measurements made at the near, centre, and far ends of the diffusion box (see Fig. 27). Furthermore, the position-dependent efficiencies were relatively flat, even at higher thresholds. At a threshold cut of 2.5 photoelectrons, the electron efficiency remained above 90% at all 3 measurement positions (see Fig. 28).

Based on the results with the first prototype, a second iteration design has been completed and will be used for the production version of the Čerenkov detector. Construction is scheduled to begin in early 2004 and further in-beam tests will be performed using the muon/pion beam lines at TRIUMF.

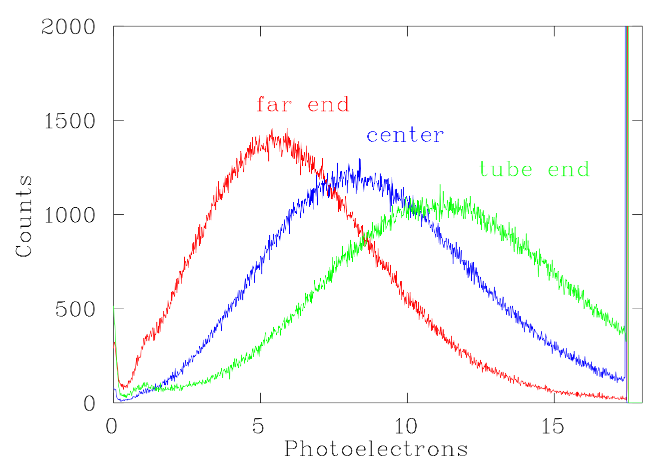

Fig. 27. Photoelectron yields for the prototype Čerenkov detector as a function of beam position.

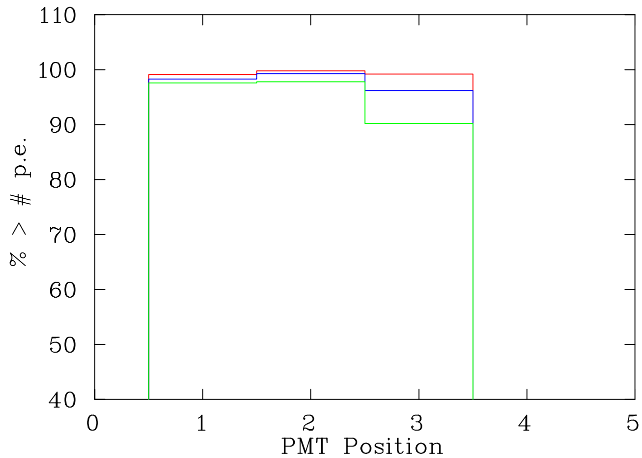

Fig. 28. Measured electron efficiencies for the prototype Čerenkov detector as a function of beam position.

Back angle support structure

Considerable effort has gone into the engineering design of a support structure for the $G\emptyset$ Čerenkov and CED arrays. Although the Canadian subgroup was initially responsible only for the design of the Čerenkov support structure, it was soon realized that the CED support structure would be closely coupled to the former due to the physical proximity of the two detector subsystems. As such, an integrated design for the two detector subsystems was pursued. The support structure centres around the use of prefabricated aluminum extrusions from Bosch because of their strength, versatility, and relatively low costs. A series of detailed finite-element analysis studies was carried out at TRIUMF, using the program ANSYS, to identify potential problems and to optimize the strength and cost of the support structure. The design consists of a second Ferris wheel type support structure, which will couple to the existing FPD support structure (also a Ferris wheel type design) and to the linear rails on the existing $G\emptyset$ detector platform. A conceptual illustration of the $G\emptyset$ backward angle configuration is shown in Fig. 29, with the superconducting magnet, the 3 detector arrays (FPD, CED, Čerenkov) in each of the 8 sectors, and their respective support structures.

Over the spring, the parts for a single octant of the support structure were procured and this subsystem was successfully assembled at TJNAF (see Fig. 30). As various components of the backward angle detectors arrived at TJNAF over the summer, work began on a test assembly of one octant of the backward angle system. Both the Canadian and French groups have supplied a mock-up Čerenkov detector for test mounting in the support structure frame. Both Čerenkov mock-ups have been test fitted and will mount as required to meet nominal design specifications. Concurrent with this work, test-fitting of the CED scintillators, lightguides, and PMTs also began. An assembly

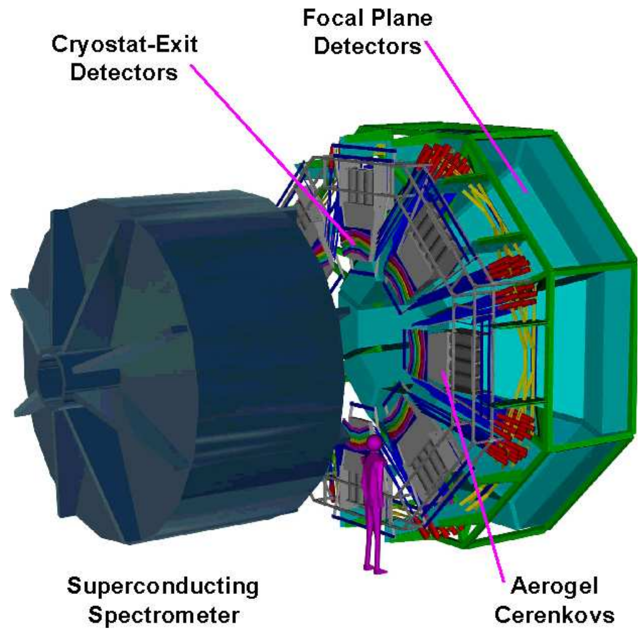

Fig. 29. Conceptual layout of the $G\emptyset$ backward angle configuration.

Fig. 30. A single octant of the back angle detector support structure.

to locate and hold the CED scintillators was designed and built. This assembly was constructed from a structural foam material, Rohacell-71, which is light-weight ($\approx$71 g/cm^3) and is easily machinable. Presently, work is under way to complete the optical and mechanical coupling of the CED scintillators to their respective lightguides. Once assembly of this first octant is successfully completed, a first set of tests using cosmic rays will be carried out at TJNAF to characterize these detectors and to help identify potential problems.

Beam line monitors

The success of the $G\emptyset$ experiment will be closely linked to the precise measurement and control of the electron beam properties. To make the subtle, refined asymmetry measurement of 1 ppm or better, the beam properties must be held within tight constraints. In pursuit of this, the beam position must be measured to better than 25 μm per 33 ms time window and the beam current to 40 ppm during the same 33 ms time window. To accomplish this, $G\emptyset$ uses two sets of XYQ microwave cavity monitors. These monitors require precision electronics designed and built by TJNAF and TRIUMF. Specifically, the position monitors produce a voltage signal based on position for the X and Y cavities, and a current proportional voltage signal for the current cavity. The voltage is amplified by dedicated amplifiers designed specifically for the dynamic range of the cavities expected during the course of the $G\emptyset$ experiment. The output from these amplifiers is fed into the TRIUMF precision voltage to frequency converters and thence into the $G\emptyset$ DAQ scalars.

One set of these XYQ cavities is installed approximately 30 m upstream of the $G\emptyset$ target. The second set of XYQ cavities is installed on the $G\emptyset$ diagnostic girder immediately before the target. Also on this girder are a pair of standard stripline beam position monitors, a pair of super-harp wire scanners, and an optical transmission view. The combination of these monitors will allow a beam position measurement of better than 10 μm per helicity window and an angle measurement of better than 0.5 μrad.

In addition to measuring and tightly controlling the beam properties, there will also be a need to determine the false asymmetries contributed by the beam parameters of position, angle, and current on target. Knowledge of the false-asymmetries is required in order to extract the physics asymmetries and its associated uncertainties. The false asymmetries are given by

$$\mathrm{A_f} = \sum \frac{\partial Y}{\partial X_i} \Delta X_i$$

where ∂Y is the change in the detector yield, ∂X_i is the change in the i^{th} beam parameter, and ΔX_i is the helicity correlated asymmetry per quartet. To calculate these false asymmetries, the sensitivities $\frac{\partial Y}{\partial X_i}$ must be measured. To accomplish this, deliberate and controlled beam modulation is introduced. This is accomplished by sending a dc current to beam steering magnets far upstream from the $G\emptyset$ target. The steering magnet positions are chosen to minimize $x - y$ motion coupling at the target. By modulating a specific beam parameter, $\{X, Y, \Theta_x, \Theta_y, E\}$, and noting the detector yield response, $\partial Y / \partial X_i$ can then be extracted. These slopes will be measured at the beginning of each data run while the helicity asymmetry will be measured continuously throughout the run. This modulation system has been tested with beam and works as expected. Shown in Figs. 31 and 32 are plots of the beam displacements resulting from modulation of the upstream steering coil.

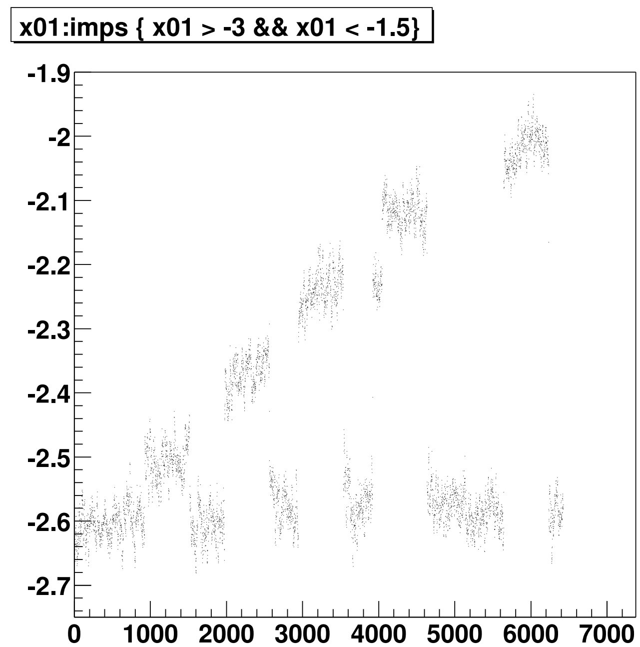

Fig. 31. Beam displacement resulting from modulation of upstream steering coils. The vertical axis gives a measure of the beam position (in mm) and the vertical axis is in units of time (macro pulse signal).

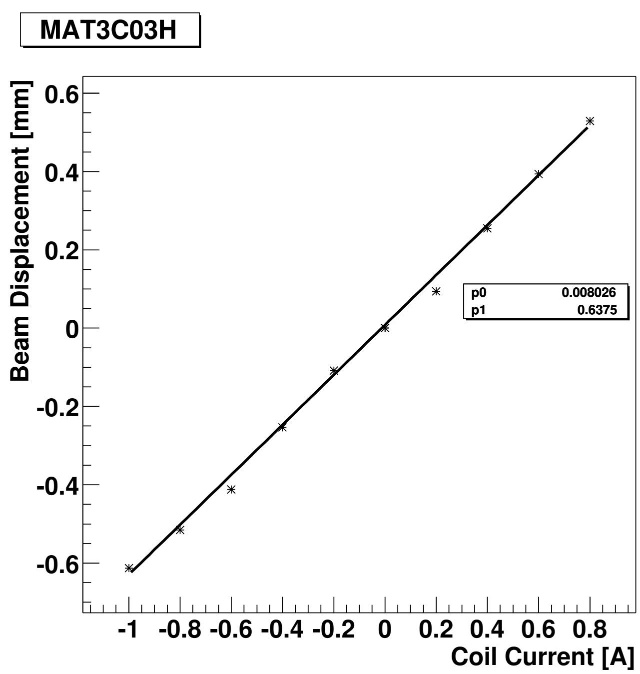

Fig. 32. Beam displacement as a function of steering coil excitation.

This modulation control system is being developed by members of the Canadian subgroup, and was tested in the $G\emptyset$ commissioning run during the fall and winter, 2002. Further developments of this system have included general beam/detector diagnostic software which allows for searches on the detector-magnet system asymmetry null coordinates, otherwise known as the sweet spot.

The 2002–2003 commissioning runs

The $G\emptyset$ experiment ran in forward angle mode from October, 2002 to January, 2003. During this period and the development period starting in August, TRIUMF, University of Manitoba and UNBC personnel staffed a total of approximately 17 person-weeks of shifts.

The equipment used is shown in Fig. 33. One can see the liquid hydrogen target service module, the 8-sector toroidal superconducting spectrometer magnet (SMS), and the focal plane detector array. During the engineering run, the magnet, target, detectors, electronics, DAQ, and software were commissioned and are operational. The principle of the forward angle measurement is shown in Fig. 34. Recoil protons at $\theta \sim 62° - 68°$ (corresponding to electrons at $15° - 5°$) are focused on the detector array in contours of constant Q^2.

Magnet (SMS) Initial manufacturing defects in the magnet were repaired in early 2002. Initially, the magnet was only run to 4500 A, but the full design current of 5000 A was reached on December 18, 2002 and this current was used for the rest of the December running period and in January, 2003.

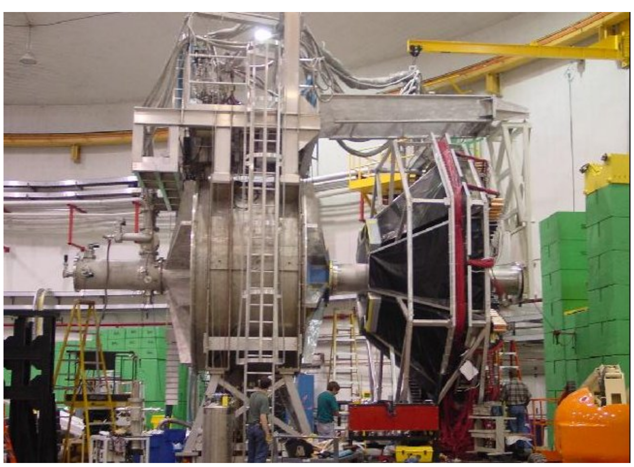

Fig. 33. Apparatus being prepared for the 2002–2003 engineering run. From left to right are the liquid hydrogen target service module, the 8-sector toroidal superconducting spectrometer magnet, and the detector array.

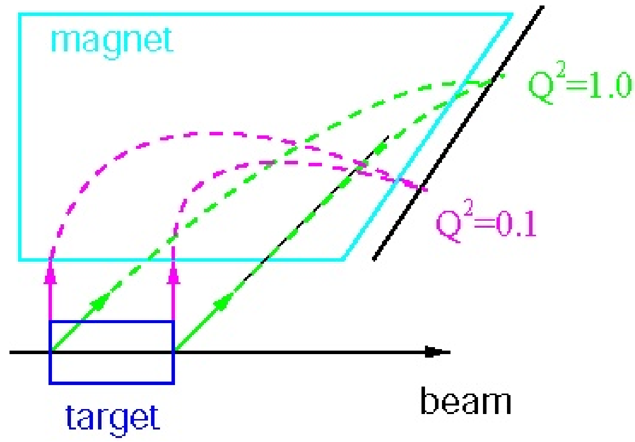

Fig. 34. A schematic of the $G\emptyset$ forward-angle configuration tested in the 2002–2003 engineering run. Recoil protons are focused on the detector array in contours of constant Q^2.

LH_2 target The $G\emptyset$ liquid hydrogen target is a 200 mm long, 6 l target. It operates at 1.7 atm and 19 K and is designed to handle 500 W without boiling. The liquid is circulated at 5.9 l/s. The target was tested at full 40 μA $G\emptyset$ beam and worked well. Figure 35 shows the $G\emptyset$ asymmetry width as a function of raster size. By reducing the raster to a very small size, it was possible to see the effects of the onset of target boiling. At the normal operating raster size there was no indication of target boiling and density fluctuations are negligible.

As discussed in more detail later, there was evidence that the downstream target window was contributing inelastic background. The target cell has been modified to reduce this background. As well, an insertable thick window has been added as a diagnostic tool.

$G\emptyset$ beam: $G\emptyset$ requires an unusual beam time structure with 32 ns between pulses. This dictates operation at 31 MHz, 1/16 the usual 499 MHz with 2 ns between pulses. To reach the desired $G\emptyset$ beam current of 40 μA, much higher charge must be in each bunch than would normally be the case, putting special demands on the ion source and on beam optics in the injector.

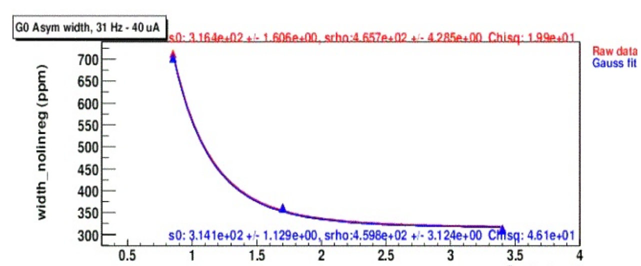

Fig. 35. The $G\emptyset$ asymmetry width in ppm as a function of the raster size in mm. Normal operation is at the right-hand end of the plot, far from any indication of target boiling.

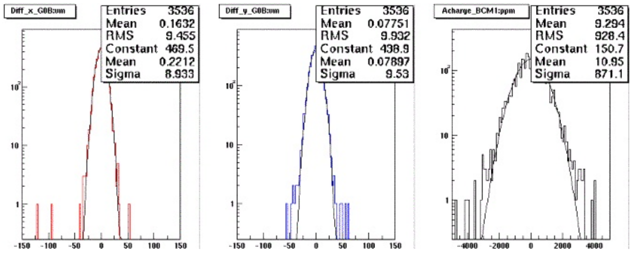

Fig. 36. Helicity-correlated beam properties measured in the 2002–2003 engineering run. From left to right, the panels show the change in x-position, y-position and beam current on helicity flip. The centroids are consistent with zero and the peak widths are $\sigma_{\Delta x} = 9\ \mu$m, $\sigma_{\Delta y} = 10\ \mu$m, $\sigma_{A_z} = 870$ ppm.

A 40 μA beam with most of the desired $G\emptyset$ properties was delivered in January, but the beam was not as stable as required, and work is continuing. Helicity correlated variations in beam properties may be reduced by use of feedback systems, some of which were tested in the 2002–2003 engineering run. In general the charge feedback system worked well, but the position feedback did not. Figure 36 shows an example of the helicity correlated position and intensity measured during the run. The goal of the beam development program is to have helicity correlated beam position differences <20 nm averaged over a 700 hour run.

Detectors and electronics For each octant, the focal plane detectors are arranged in 16 pairs of arc-shaped scintillators, each arc following a curve of constant Q^2. Front-back coincidences eliminate neutrals. All detectors, electronics and data acquisition were tested and worked well. It was found, however, that there was an unexpectedly large low energy background which was below the discriminator threshold but which increased the anode currents in the photomultiplier tubes. Shielding around the beam line has now been modified to reduce this background and the gains of the affected photomultiplier tubes have been reduced to further decrease their anode currents.

In the forward angle configuration, time of flight is used to separate the desired elastically scattered protons from pions and inelastic protons. Figure 37 shows a time-of-flight spectrum from one of the focal plane detectors (detector 8). The pion peak is cleanly separated from the elastic peak, but a tail of the inelastic proton peak extends under the elastic proton peak. This causes a dilution of the asymmetry which must be corrected for. Simulations suggest that the inelastic peak contains important contributions from the downstream target window. As mentioned in the target section, the target cell has been modified to reduce this background.

Asymmetry data In January the experiment was able to take some asymmetry data at 40 μA beam current. Although only 51 hours of data were accumulated, clear negative value was already evident.

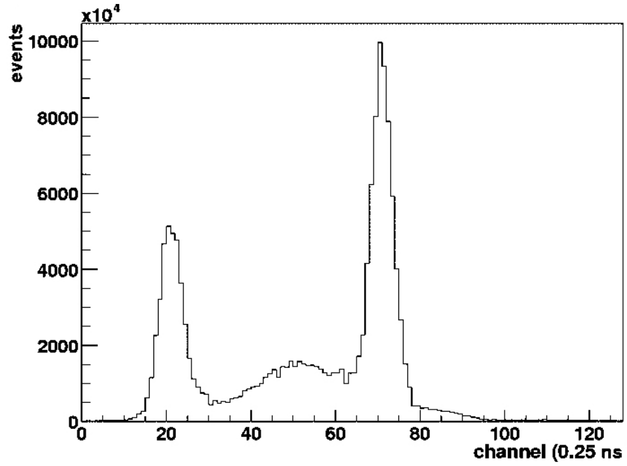

Fig. 37. A time-of-flight spectrum taken from one focal plane detector (detector 8). From left to right the peaks are pions, inelastic protons and elastic protons. The asymmetry measured for the elastic peak must be corrected for dilution by the tail of the inelastic peak.

Future In late 2003, a second commissioning/engineering run commenced and will continue into early 2004. Upon completion of this run, the forward angle production running will begin, with 700 hours of good data expected. Back angle production running is planned for 2004–2006.

Canadian subgroup of the $G\emptyset$ collaboration: J. Birchall, W.R. Falk, M. Froese, Z. Ke, L. Lee, S.A. Page, W.D. Ramsay, A. Rauf, G. Rutledge, M.J. Steeds, W.T.H. van Oers (Manitoba); E. Korkmaz, T. Porcelli (UNBC); C.A. Davis (TRIUMF).

TJNAF Experiment 02-020

$\mathbf{Q^p_{weak}}$: a search for new physics at the TeV scale via a measurement of the proton's weak charge

(J. Birchall, W.R. Falk, L. Lee, S.A. Page, W.D. Ramsay, W.T.H. van Oers, Manitoba; E. Korkmaz, T. Porcelli, UNBC; J. Doornbos, TRIUMF)

Introduction

A major new initiative, the $\mathrm{Q_{weak}}$ experiment [TJNAF proposal E-02-020], is under rapid development at Thomas Jefferson National Accelerator Facility (Jefferson Lab), a premier electron scattering facility for nuclear and particle physics. The $\mathrm{Q_{weak}}$ experiment will measure the proton's weak charge to high precision, in turn providing a precise measurement of the weak mixing angle $\sin^2(\theta_W)$ at low energy, which can be compared to data from high energy collider experiments at LEP and SLC. The $\mathrm{Q_{weak}}$ experiment is moving forward on an aggressive construction schedule with the aim of installing equipment in Jefferson Lab's Hall C by 2007. One member of the Canadian group (S.A. Page) is a Co-Spokesperson for the experiment, while another (W.T.H. van Oers) leads the team building the magnetic spectrometer, the coils of which are to be constructed with NSERC funds, under project management provided by TRIUMF.

Physics motivation

Precision tests continue to play a central role in elucidating the nature of the electroweak interaction. Existing experimental data provide impressive constraints both on the standard model and on proposed scenarios for extending it. Measurements at the Z^0 pole have constrained the weak mixing angle $\sin^2(\theta_W)$ to impressive precision at that energy scale. However, a precision experimental study of the evolution of the weak mixing angle to lower energies has not yet been successfully carried out. The standard model evolution predicts a shift of $\Delta \sin^2(\theta_W) = +0.007$ at low Q^2 with respect to the Z^0 pole best fit [Particle Data Group] value of 0.23113 ± 0.00015 (Fig. 38). This gives rise to a firm prediction of the proton's weak charge, $Q_{\rm wp} = 1 - 4\sin^2(\theta_W)$, based on the running of the weak mixing angle, corresponding to a 10σ effect in our experiment.

Figure 38 shows the standard model prediction in a particular scheme[1] for $\sin^2(\theta_W)$, together with existing and proposed world data. As is seen from the figure, the very precise measurements near the Z^0 pole set the overall magnitude of the curve; to test its shape one needs precise measurements at other energies. Currently, there are only two other experiments which test the evolution of $\sin^2(\theta_W)$ to lower energy scales at a significant level – one in the Colorado atomic parity violation[2] (APV) experiment on cesium, and one from the NuTeV high energy neutrino-nucleus scattering experiment at Fermilab, showing a 3σ deviation *above* expectations. However, both of these results suffer from complications in theoretical interpretation which limit their physics impact. In contrast, the $\mathrm{Q_{weak}}$ experiment at Jefferson Lab will be performed with much smaller statistical and systematic errors, and has a much cleaner theoretical interpretation. The dominant hadronic effects that must be accounted for in extracting $Q_{\rm wp}$ from the data are contained in form factor contributions that can be sufficiently constrained by the current program of parity violating electron-proton scattering measurements under way at Jefferson Lab and elsewhere, without reliance on theoretical nucleon structure calculations.

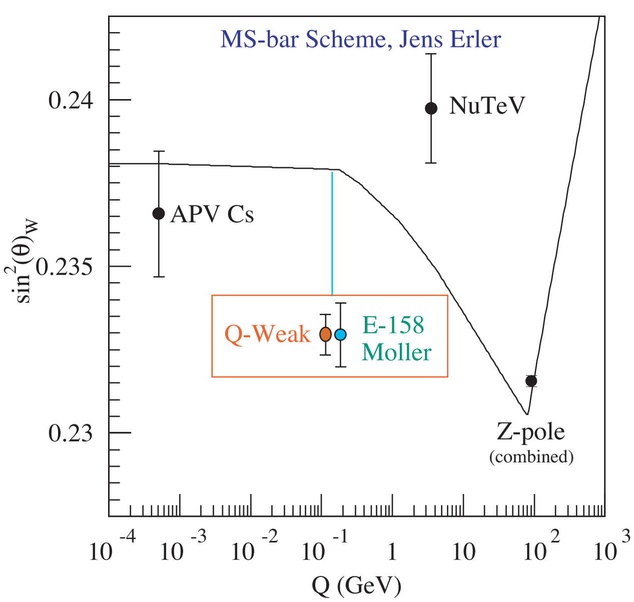

Fig. 38. Calculated running of the weak mixing angle in the standard model. Data points are from the atomic parity violation experiment on Cs, the NuTeV experiment, and from experiments at the Z^0 pole. Also shown are anticipated error bars for $\mathrm{Q_{weak}}$ and the Møller experiment at SLAC.

M.J. Ramsey-Musolf, A. Kurylov and J. Erler have carried out an extensive review of theoretical uncertainties that affect the prediction of $Q_{\rm wp}$ itself, independent of nucleon structure contributions. Adding these uncertainties in quadrature gives a "theoretical" uncertainty of ± 1.9 % in $Q_{\rm wp}$, as compared to the anticipated total uncertainty of $\pm 4\%$ for the $\mathrm{Q_{weak}}$ experiment.

We would like to emphasize that this new experiment is an essential element of a program of very sensitive low energy tests of the standard model that is complementary to other efforts under way or planned world wide. Erler, Kurylov and Ramsey-Musolf demonstrated that a measurement of $Q_{\rm wp}$ at the $\pm$ 4% level probes new physics at energy scales up to 4.6 TeV [Erler *et al.*, Phys. Rev. **D68**, 016006 (2003)]. It should also be noted that the $\mathrm{Q_{weak}}$ experiment is complementary to an experiment under way at SLAC (E158) to measure the weak charge of the electron and infer the weak mixing angle from parity violating electron-electron (Møller) scattering, but which is currently not expected to reach a similar precision in $\sin^2(\theta_W)$.

The experiment

The $\mathrm{Q_{weak}}$ collaboration will carry out the first precision measurement of the proton's weak charge,

[1] Note that $\sin^2(\theta_W)$ is not strictly an observable, but depends on what has been absorbed into the definition and what has been corrected for. Figure 38 shows a recent calculation by Erler, Kurylov and Ramsey-Musolf, details of which are given in Erler *et. al.* [Phys. Rev. **D68**, 016006 (2003)].

[2] The interpretation of the APV result changes from agreement with the standard model to as much as a 2.6σ deviation *below* the predicted value, depending on what is included in the atomic theory calculations.

$Q_{\mathrm{wp}} = 1 - 4\ \sin^2(\theta_W)$ by measuring the parity violating asymmetry in elastic electron-proton scattering at very low momentum transfer:

$$A = (\sigma_+ - \sigma_-)/(\sigma_+ + \sigma_-) = Q^2\ Q_{\mathrm{wp}} + Q^4\ B(Q^2)$$

where σ_+ and σ_- are cross sections for positive and negative helicity incident electrons, and $B(Q^2)$ is a hadronic form factor contribution. The results of earlier experiments in parity violating electron-proton scattering will be used to constrain hadronic corrections to the data. A 2200 hour measurement of the parity violating asymmetry in elastic electron-proton scattering at a momentum transfer of $Q^2 = 0.03$ (GeV/c)^2 employing 180 μA of 80% polarized beam on a 35 cm liquid hydrogen target will determine the proton's weak charge with 4% combined statistical and systematic errors; this in turn implies a determination of $\sin^2(\theta_W)$ at the ±0.3% level at low energy. As a standalone measurement of $\sin^2(\theta_W)$, the $\mathrm{Q_{weak}}$ experiment is competitive with any channel measured in the recently completed SLD and LEP programs at the Z resonance.

A sketch showing the layout of the experiment is given in Fig. 39. A longitudinally polarized electron beam, a liquid hydrogen target, a room temperature toroidal magnetic spectrometer (QTOR), and a set of detectors for the scattered electrons at forward angles are the key elements of the experimental apparatus. The toroidal magnetic field will focus elastically scattered electrons onto a set of 8 rectangular quartz Čerenkov detectors coupled to photomultiplier tubes,

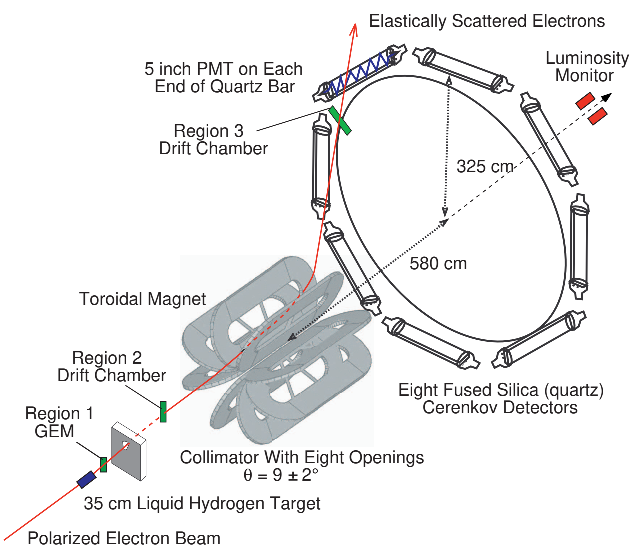

Fig. 39. Layout of the $\mathrm{Q_{weak}}$ experimental apparatus, showing the target, collimation, magnet coils and detectors for the eight identical octants of the spectrometer system. Incorporated in the apparatus is a tracking system to be used in ancillary measurements at very low beam current to map the Q^2 response of the detector system.

which will be read out in current mode to achieve the high statistical precision required for the measurements. A new high power cryotarget is under development for these measurements. The acceptance averaged asymmetry in our design is –0.3 ppm; we will measure this asymmetry to ±1.9% statistical and ±1.7% systematic errors.

The main technical challenges result from the small expected asymmetry of approximately –0.3 ppm, and the required accuracy of ±4%. The optimum kinematics corresponds to an incident beam energy of $\mathrm{E_0} =$ 1.165 GeV, scattered electron polar angles $\theta_e = 9.0 \pm 2.0°$, and azimuthal detector acceptance as large as possible (8 electron detectors with acceptance $\Delta\phi_e = \pm 15°$ each). Also, the high statistical precision required implies high beam current (180 μA), a long liquid hydrogen target (35 cm) and a large-acceptance detector operated in current mode. Radiation hardness, insensitivity to backgrounds, uniformity of response, and low intrinsic noise are criteria that are optimized by the choice of quartz Čerenkov bars for the main detectors.

It is essential to maximize the fraction of the detector signal (total light output in current mode) arising from the electrons of interest, and to calibrate both the dilution factor due to background and the detector-signal-weighted $< Q^2 >$ in order to be able to extract a precise value for $\sin^2(\theta_W)$ from the measured asymmetry. This information will be extracted from ancillary measurements at low beam current, in which the quartz Čerenkov detectors are read out in pulse mode and individual particles are tracked through the spectrometer system using a set of wire chambers. The tracking system will be capable of mapping the $< Q^2 >$ acceptance in two opposing octants simultaneously; chambers will be mounted on a rotatable wheel assembly so that the entire system can be mapped in 4 sequential measurements. A small "mini-toroid" magnet will be installed downstream of the first collimator to sweep low energy Møller electrons out of the acceptance of the middle tracking chambers (not shown in Fig. 39; this will not significantly affect the optics for the elastic electrons of interest for $\mathrm{Q_{weak}}$). The front chambers are based on the CERN GEM design and will have a fast time response (< 50 ns) and resolution of order 250 μm. The chambers plus trigger scintillator system will be retracted during normal $\mathrm{Q_{weak}}$ data-taking at high current.

Systematic errors are minimized by construction of a symmetric apparatus, optimization of the target design and shielding, utilization of feedback loops in the electron source to null out helicity correlated beam excursions, careful attention to beam polarimetry, and by carrying out ancillary measurements to determine the system response to helicity correlated beam properties and background terms. The electron beam polarization must be measured with an absolute uncertainty in the 1–2% range; at present this can be achieved in Hall C using an existing Møller polarimeter, which can only be operated at currents below 10 μA. A major effort to design and build a Compton polarimeter in Hall C at Jefferson Lab is under way as part of the laboratory's support of this and other experiments where precise beam polarimetry is an issue; the Compton polarimeter will provide a continuous on-line measurement of the beam polarization at full current (180 μA) which would otherwise not be achievable.

As noted earlier, the parity-violating asymmetry that we measure will contain contributions from nucleon structure form factors:

$$A = (\sigma_+ - \sigma_-)/(\sigma_+ + \sigma_-) = Q^2\, Q_{\rm wp} + Q^4\, B(Q^2),$$

which can be re-expressed as:

$$A = A_{Q_{\rm wp}} + A_{nff} + A_{\rm axial} = -0.19 - 0.09 - 0.01 \ \text{ppm},$$

where the first term involves the quantity of interest, the second term involves electromagnetic and strange nucleon form factors and reduces to $Q^4\, B(Q^2)$ at low Q^2, and the third term involves the eN axial form factor G_A^e.

The term A_{nff} can be constrained from the anticipated results of parity-violating electron scattering experiments that are either under way or planned over the next few years. Since these are performed at higher momentum transfers than $Q_{\rm weak}$, the results must be extrapolated to the value of A_{nff} at our Q^2. In our analysis, we consider the published uncertainty from the HAPPEX experiment [Aniol *et al.*, Phys. Lett. **B509**, 211 (2001)] together with the expected uncertainties from HAPPEXII [TJNAF E-99-115 (K.S. Kumar and D. Lhuillier, spokespersons)] and the forward angle running of $G\emptyset$ [TJNAF E-00-006 (D.H. Beck, spokesperson)]. For the extrapolation, we assume conventional dipole and Galster parametrizations for the electric and magnetic proton and neutron form factors. The fractional uncertainty in A_{nff} is $\pm 4.0\%$ at $Q^2 = 0.03$ GeV^2; since A_{nff} contributes 40% to the parity violating asymmetry in our kinematics, this leads to a systematic uncertainty of 1.6% arising from our knowledge of nucleon form factors. The axial contribution, $A_{\rm axial}$, depends on the eN axial-vector form factor G_A^e. The anticipated absolute error on the extrapolated value of G_A^e at $Q^2 = 0.03$ GeV^2 will be ± 0.25. Since this term makes a 5% contribution to the overall asymmetry, it contributes 1.2% to the systematic error in A. The quadrature sum of the two nucleon form factor errors is thus 2%.

The $\mathbf{Q_{weak}}$ magnetic spectrometer

A key component of the apparatus is a magnetic spectrometer QTOR, whose toroidal field will focus elastically scattered electrons onto a set of eight rectangular quartz Čerenkov detectors. The main requirement for the spectrometer is to provide a clean separation between elastic and inelastic electrons so that a detector system of reasonable size can be mounted at the focal plane to measure the elastic asymmetry with negligible contamination from inelastic scattering and other background processes. The axially symmetric acceptance in this geometry is very important because it reduces the sensitivity to a number of systematic error contributions.

The $\mathrm{Q_{weak}}$ magnetic spectrometer working group has designed a new resistive toroidal spectrometer with 8-fold symmetry to meet the needs of the experiment. The coil geometry has been optimized in a series of simulation studies using GEANT plus numerical integration over the conductor's current distributions to determine the magnetic field. The simplest and least expensive QTOR coil design that meets the needs of the $\mathrm{Q_{weak}}$ experiment is a simple racetrack structure with a layout shown in Fig. 40.

The QTOR magnet working group consists of scientists and engineers from the University of Manitoba, TRIUMF, MIT, Jefferson Lab, and Louisiana Technical University, led by W.T.H. van Oers (Manitoba). The Canadian group, via the University of Manitoba and TRIUMF, received funds in last year's NSERC competition to fabricate the 8 water-cooled conducting coils; the hollow copper conductor has been purchased by Jefferson Lab, which is also providing the power supply and services; the spectrometer support structure will be jointly engineered and built by MIT-Bates and Jefferson Lab.

With the conceptual design of the spectrometer essentially complete almost a year ago, our attention turned to further optics studies and simulation work to establish geometrical tolerances for coil fabrication and

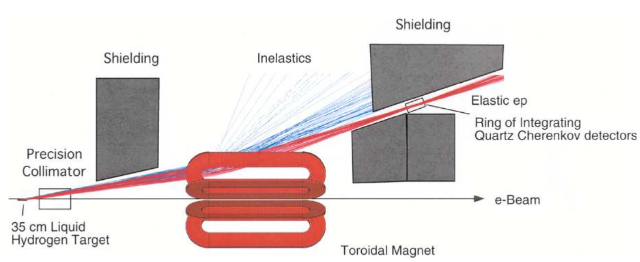

Fig. 40. Cutaway view of the experiment, showing the target, collimation, shielding, electron trajectories, and detectors for one of the eight identical octants of the spectrometer system. Elastically scattered electrons (red tracks) focus on the detectors while inelastically scattered electrons (blue tracks) are swept away by the toroidal magnetic field.

alignment. A GEANT Monte Carlo simulation package has been used to study the effects of coil misalignments on the Q^2 distribution at the focal plane as well as on the symmetry of the 8-octant system as required for systematic error reduction. Tolerances on the positioning of the QTOR magnet as a whole as well as on individual coils within the magnet have been set as a result of these studies.

A beam's eye view of the magnet, collimator, and detector systems is shown schematically in Fig. 41 with simulated GEANT events. Scattered electrons in the range 7–11° are selected by a double collimator system. Photons project an image of the primary collimator onto a plane downstream at the magnet focus; inelastic electrons are deflected to larger angles, out of the acceptance of the detector bars. The nonideality of the 8-coil toroidal field leads to a distortion of the elastic event distribution at the focal plane, with drooping edges that we refer to as a "moustache". The collimator shape plays a key role in defining the shape of the elastic event band accepted by the detectors, i.e. in "trimming the moustache", which is important for minimizing the sensitivity to helicity-correlated beam motion, magnet alignment errors, and related systematic effects.

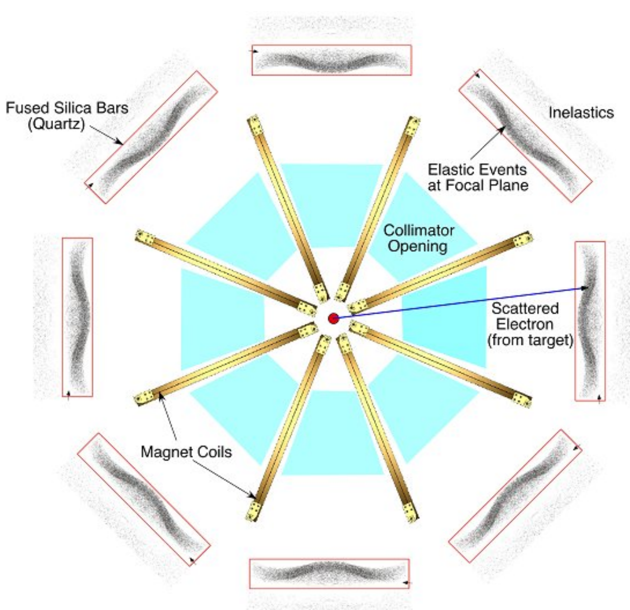

Fig. 41. Beam's eye view with simulated GEANT events. The magnet coils, primary collimator openings, and quartz detector bars are indicated. Elastic events are focused in θ and defocused in ϕ along the width and length of the detector bars, respectively. Inelastic events are deflected to larger angles, outside the detector boundaries.

Magnetic field verification

Acceptance tests of the assembled magnet of the QTOR spectrometer must guarantee that the desired Q^2 interval of the scattered electrons for each sector is properly focused on the quartz Čerenkov detectors. A magnetic field mapping apparatus, built by the Canadian group for the $G\emptyset$ experiment[3], will be employed to map the QTOR spectrometer field. It is currently located at UIUC (Fig. 42); we will retrofit the field mapper and move it first to MIT-Bates and later to Jefferson Lab for mapping the QTOR spectrometer.

Much effort went into the design, construction and commissioning of the $G\emptyset$ field mapping system at TRIUMF, the University of Manitoba and the University of Northern BC. The system is capable of providing an absolute position determination of ±0.2 mm, and a field determination of ±0.2 G, in order to resolve a zero-crossing position to within ±0.3 mm. The field mapping system consists of a programmable gantry with full 3D motion within a $(4\times4\times2)$ m^3 volume, and a set of high precision Hall probes, thermocouples and clinometers (which measure tilt angle) mounted on the end of a probe boom on the gantry. Because the coils of the $G\emptyset$ magnet were completely encased in a cryogenic vacuum vessel, the field mapping had to determine the coil location by a very accurate measurement of the zero crossing of selected field components of the fringe field. Since the Q_{weak} magnet is open, the main magnetic field can be mapped directly. For the Q_{weak} mapping, new Hall probes with the appropriate dynamic range will be installed.

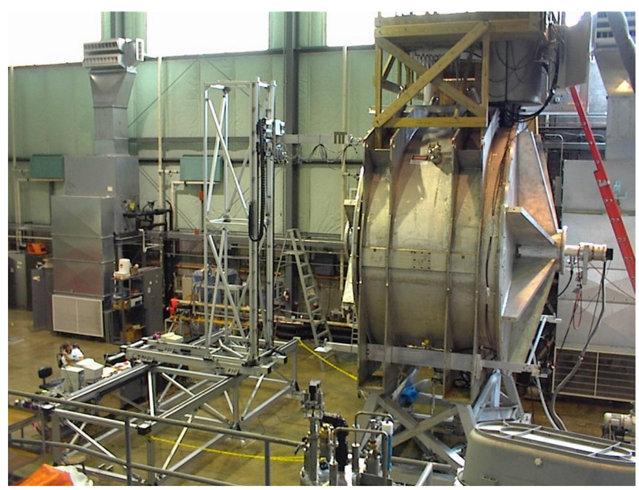

Fig. 42. Magnetic field mapper, on location at UIUC for mapping the $G\emptyset$ magnet.

[3]The $G\emptyset$ magnet is an 8-coil superconducting toroidal spectrometer of a similar size to QTOR. Magnetic field mapping for $G\emptyset$ posed a particular challenge since the coils were completely encased in a cryogenic vacuum vessel.

Simulation studies: systematic errors

The Canadian group's simulation effort builds on expertise gained from TRIUMF Expts. 497 (Measurement of parity violation in $\vec{p}-p$ scattering at 221 MeV) and 704 (Measurement of charge symmetry breaking in $np \to d\pi^0$ close to threshold) as well as from the ongoing $G\emptyset$ experiment at Jefferson Laboratory. We are concentrating initially on the study of systematic errors that result from beam properties that change when electron beam helicity is reversed. Initial estimates that were made to set requirements on beam properties at the time of the experimental proposal were based on a simple geometrical model in which the acceptance of the detectors was set by the primary collimator. Systematic error estimates have now been made based on detailed Monte Carlo calculations that track electrons from the target, through the collimators and magnetic field to the detectors.

Helicity correlations in the beam parameters can lead to false parity asymmetries. The measured parity asymmetry, $A_{\rm meas}$, is written in terms of the physics asymmetry, $A_{\rm phys}$, in the following way for sufficiently small helicity correlations:

$$A_{\rm meas} = A_{\rm phys} + \sum_{i=1}^{n} \Big(\frac{\partial A}{\partial S_i}\Big)\delta S_i,$$

where beam parameter S_i changes on helicity reversal to $S_i^{\pm} = S_i \pm \delta S_i$. The detector sensitivities $\partial A/\partial S_i$ can be determined preferably by deliberate modulation of the relevant beam parameter or from natural variation of beam parameters. The helicity-correlated beam parameter differences, δS_i, are measured continuously during data-taking. The goal is to constrain systematic uncertainties from each source to be no more than the statistical uncertainty on the measurement of the parity asymmetry, i.e., no more than 6×10^{-9}, and that corrections should be accurate to 10%.

A perfectly symmetric detector system, magnet and collimator aligned precisely with the beam should be insensitive to small modulations of beam position on helicity flip. If the beam is moved away from this "position neutral axis", however, symmetry is broken and false parity-violating effects are seen. To study this, the Q^2-weighted event rate, $N(x,y)$, seen by a Čerenkov bar is mapped out as a function of the position of the beam on target and of displacement of the magnetic field. It is then possible to estimate the false parity asymmetry due to beam motion on helicity flip and to set tolerances on the positioning of the magnet. Tolerances break down into dc properties, that is, average values for beam parameters, and helicity-correlated changes. A large beam raster size (4 mm in place of 2 mm) decreases the possibility of spurious results due to bubbling of the target, so systematic errors were estimated for 4 mm and 2 mm rasters.

Likewise, the sensitivity to beam size modulation has been explored. The effects of the size modulation are diluted by the rastering if there is no correlation of the rastering with helicity. For a false asymmetry of 6×10^{-9}, the rastered beam should contain a size modulation no larger than about 2 nm. As the angle of incidence of the beam on target is changed, so the range of Q^2 accepted by the collimators changes and with it the event rate. There is in addition a variation of effective thickness of the target, but the effect is small compared with the variation of cross section and is, in any case, removed by normalization to the luminosity monitors. The systematic error requirement becomes $|\theta_0\delta\theta_0| \leq 6.3\times 10^{-6}$ mrad^2, corresponding to a dc offset of the angle of beam on target of about 60 μrad when $\delta\theta_o = 100$ nrad.

Spectrometer calibration efforts, Q^2 distribution and tracking

Through our heavy involvement in the design, construction, and field mapping of the QTOR magnetic spectrometer, the Canadian group plans to participate significantly in the spectrometer calibration and tracking effort of the collaboration. It should be noted that we must determine $< Q^2 >$ to 1% to meet the goals of our experiment; since hadronic corrections to the asymmetry are proportional to Q^4, we must also determine the Čerenkov-light-weighted average of this quantity in order to analyze the asymmetry data. It is clear that a thorough understanding of the spectrometer system and the shape of the light-weighted Q^2 distribution for elastic electrons at the focal plane is an essential ingredient to the success of this experiment. Work is proceeding on two fronts: simulations of the spectrometer tracking system and main detector response to predict the shape of the Q^2 observed distribution, and subsequent optimization of the calibration, alignment and tracking systems that will lead to measurements of this distribution under experimental conditions.

Experiment status

Following initial PAC approval in 2002 and a successful technical review in January, 2003, a funding package to support the equipment construction totalling approximately US$3.4 M has been put in place, provided by Jefferson Lab, the US DOE, NSF, and NSERC, Canada. The experiment is on a fast track for construction and installation in Hall C at Jefferson Lab by 2007. Bids for construction of the magnetic spectrometer coils, which are the responsibility of the Canadian subgroup, will be solicited in early 2004, with initial assembly and field mapping planned to take place at MIT-Bates in 2005.

The Q_{weak} collaboration

The Q_{weak} collaboration consists of 51 scientists from 17 institutions. The principal Spokesperson is R.D. Carlini (Jefferson Lab) with Co-spokespersons J.D. Bowman (LANL), W.M. Finn (William and Mary), S. Kowalski (MIT), and S.A. Page (Manitoba). G.R. Smith (Jefferson Lab) is the Project Manager. Major stakeholders in the experiment are Jefferson Lab, who will provide the polarized beam, the target, the beam line instrumentation, and required shielding; Los Alamos National Lab, who lead the design and construction of the detector package and associated electronics; Louisiana Tech, who lead the effort in computer simulations and are building the forward GEM tracking detectors; MIT, who play a major role in the design and construction of the spectrometer support stand and the Compton polarimeter project, the Canadian collaboration (Manitoba, UNBC, TRIUMF) who are leading the magnetic spectrometer project, and a consortium of US university groups including The College of William and Mary, Louisiana Tech, and Virginia Polytechnic University, who have taken responsibility for the spectrometer calibration and particle tracking system. The major stakeholders are represented by an Institutional Council, which is the decision-making body regarding policy issues for the experiment. The council holds regular meetings by telephone conference to monitor the status of institutional construction projects and contributions to the experiment. S.A. Page is currently serving as Chair of the Institutional Council.

List of Q_{weak} collaborators: M.J. Ramsey-Musolf, Caltech; D. Armstrong, T. Averett, W.M. Finn, K.H. Grimm, College of William and Mary; C. Keppel, Hampton University; R.D. Carlini, S. Chattopadhyay, R. Ent, D.J. Gaskell, A. Lung, D. Mack, S. Majewski, H. Mkrtchyen, M. Poelker, J. Roche, G.R. Smith, S. Wood, C. Zorn, Jefferson Lab; J.D. Bowman, G. Mitchell, S. Penttila, W.S. Wilburn, Los Alamos National Lab; T. Forest, K. Johnston, N. Simicevic, S. Wells, Louisiana Technical University; J.A. Dunne, Mississippi State University; S. Kowalski, R. Suleiman, S. Taylor, MIT; A.K. Opper, Ohio University; C.A. Davis, J. Doornbos, TRIUMF; J. Erler, Universidad Nacional Autonoma de Mexico; R. Jones, K. Joo, University of Connecticut; J. Birchall, W.R. Falk, L. Lee, S.A. Page, W.D. Ramsay, W.T.H. van Oers, University of Manitoba; F.W. Hersman, M. Holtrop, H. Zhu, University of New Hampshire; E. Korkmaz, T. Porcelli, University of Northern BC; C. Hagner, N. Morgan, M. Pitt, Virginia Polytechnic Institute. Experiment status: in preparation.